EXPERIMENTAL INVESTIGATION OF OILFILM BEHAVIOUR IN SHORT JOURNAL BEARINGS

Thesis by

Boris Auksmann

In Partial Fulfillment of the Requirements
For the Degree of

Mechanical Engineer

California Institute of Technology

Pasadena, California

1959

ACKNOWLEDGMENTS

The author wishes to express his sincere thanks to Dr. A. J. Acosta for his guidance and contributions during the course of this investigation. He is also grateful to Dr. D. S. Wood for his assistance in solving the engineering problems encountered during apparatus design, to Mr. C. T. Eastvedt for his advice and assistance in photographic recording of the cavitation phenomena and to Mrs. R. D. Toy for proofreading the final draft of the thesis.

ABSTRACT

This report contains the description of the test apparatus that was designed and built for experimental investigation of oilfilm behaviour in short full-journal bearings of circumferential feed groove type. An account of the engineering problems solved in connection with the design and development of the apparatus is also given.

Complete pressure distributions were obtained for a two inch diameter, one inch long bearing operating at 3500 rpm under 30 and 60 lb. applied loads and with various axial pressure gradients and supply pressures. The results are presented in graphical form and a comparison is made with the short bearing theory developed by F. W. Ocvirk. Agreement with theory was found to be very good when operating with low axial pressure gradient and high supply pressure (cavitation completely suppressed), while with high axial pressure gradient substantial differences in pressure distribution were found.

Visual observations of oilfilm behaviour were made with a transparent plastic bearing of the same proportions, operating with a 60 lb. load at 3500 rpm. Cavitation behaviour under various axial pressure gradients and supply pressures is discussed, and photographic records of typical cavitation behaviour are presented in the report.

Eccentricity and attitude angle measurements were made in all tests and experimental results are presented with pressure distribution data and cavitation behaviour records.

TABLE OF CONTENTS

SYMBOLS

C_R	radial clearance, in.
d	journal diameter, in.
e	eccentricity of journal and bearing axes, in.
h	Local fluid film thickness, in.
ℓ	bearing length, in.
ℓ/d	length diameter ratio
n	eccentricity ratio or attitude = e/C
P	applied load, lb.
P_X , P_Y	components of applied load parallel and normal to line of center of journal and bearing, lb.
P_S	supply plenum pressure lb./sq. in.
P_D	discharge plenum pressure lb./sq. in.
p	local fluid film pressure, lb./sq. in.
Re	Reynolds number = $\frac{U \cdot C_R}{\mu/\rho}$
r	bearing radius, in.
U	surface speed of journal, in./sec.
x, y, z	coordinates
θ	angle measured from maximum film thickness
μ	absolute viscosity of lubricant centipoises/(6.9×10^6), except as noted
Φ	attitude angle, angle between the load line and line of centers of journal and bearing, degrees
ρ	density lb./cu. in.

I INTRODUCTION

Theoretical solutions for oilfilm behaviour in short journal bearings have been worked out by many people. Most investigators have based their pressure distribution functions on approximate solutions of Reynold's equation, i.e.,

$$\frac{\partial}{\partial x}\left(h^3\frac{\partial p}{\partial x}\right) + \frac{\partial}{\partial z}\left(h^3\frac{\partial p}{\partial z}\right) = 6\mu U\frac{\partial h}{\partial x}$$

by neglecting the first term on the left side of the equation as being small compared to the other terms. These solutions can be applied to bearings with central oil supply holes, with axial oil feed grooves or with circumferential oil feed grooves by applying appropriate boundary conditions to the solution.

The theoretical solutions so obtained have been compared with experimental data for a bearing with central oil supply hole or axial oil feed groove by several investigators (1)(2)(3)* with various degrees of agreement. Although these theoretical solutions indicate a positive and a negative pressure region with respect to datum** pressure in a journal bearing oilfilm, the experimental data are available for the positive pressure region only, while the negative pressure region is assumed to be nonexistent in practical applications. The lack of the negative pressure region is usually explained by assuming that cavitation

---

* Numbers in parenthesis indicate references at the end of the text.

** Datum pressure is defined as the line of symmetry for a particular circumferential pressure distribution curve.

breaks up the diverging oil film and relieves negative pressures at the vapor-pressure level of the lubricant (3). Ocvirk limits the cavitation assumption to the cases of low (atmospheric) datum pressures and states that in practice the total load is carried by the positive pressure region only (1). Although the cavitation phenomenon is a plausible explanation of why negative pressure regions are not observed in practice, conclusive experimental proof of the correctness of this assumption for conditions of elevated plenum (datum) pressures and for applications with large imposed axial gradient is still lacking. For example, a theoretical solution by Wannier (4), indicating possibility of reverse flow in divergent film region and thereby a reduced load carrying capacity, offers an alternative explanation. However this point is still somewhat open as extensive calculations of Wannier's theory are not available for comparison with experimental data.

There is very little experimental data available about the oilfilm behaviour in a bearing with circumferential oil feed groove. To the author's knowledge,no comparison of existing theoretical solutions has so far been attempted with experimental data for a bearing of the above type operated with high axial pressure gradients or at elevated datum pressures. However, in bearings with circumferential oil feed grooves, a relatively high axial gradient is often present in practical applications, particularly where high supply pressures are used. High axial gradient will result in high datum pressures at least in the regions near the feed groove, with the resulting implication that in such bearings at least part of the load is carried by negative pressure region. Cavitation, if it

occurs, should be limited to the regions furthermost from the feed groove. In special applications where submerged bearings are used in pressurized environment, high datum pressures may be present in the entire bearing; hence cavitation should not occur and positive as well as negative pressure regions, predicted by theoretical solutions, should be present. Theoretically then, a pressurized journal bearing would have twice the load carrying capacity, provided the assumption about cavitation is correct. On the other hand, if low pressure region, shown by theoretical solutions, is relieved by reverse flow phenomena as suggested by Wannier's theory, then negative pressure region should be nonexistent even at high axial gradients and/or datum pressures.

In mechanical engineering practice short journal bearings of circumferential feed groove type are particularly well suited for applications where load orientation cannot be fixed (axial feed groove bearings can be fed only from the low pressure side) and compact dimensions with efficient cooling are required. Because of the above characteristics, this type of bearing has been extensively used in internal combustion engines and other high speed rotating machinery working with large bearing loads.

In recent years there has been a strong development trend towards higher power to weight ratios in the rotating machinery field. This has resulted in more efficient utilization of engineering materials, in going to higher rotation speeds and in the need for bearings with optimum performance characteristics for each particular application. A well

developed theory applicable to circumferential feed groove journal bearings, and substantiated by experimental data would be a powerful tool for designing journal bearings with optimum performance characteristics for a wide variety of operating conditions.

With these ideas in mind, it was felt that an experimental investigation of oilfilm behaviour in short journal bearings of the circumferential feed groove type would serve a twofold purpose:

1. Provide experimental data about oilfilm behaviour (in terms of known parameters) which could be used for comparison with existing theoretical solutions applicable to short bearings.

2. Provide information about the oilfilm behaviour in the cavitation region, if any, in such bearings in order to obtain a better model for the flow there.

At this stage a decision was made to design and build an experimental apparatus which would enable one to:

1. Observe oilfilm behaviour visually in order to determine the presence and nature of cavitation in the oilfilm, and possibly also the flow pattern.

2. Measure pressure distribution in circumferential as well as in axial direction.

3. Measure journal eccentricity.

4. Vary the imposed axial pressure gradient as well as the datum pressure in order to determine their effect on the oilfilm behaviour.

5. Measure torque or at least the torque variations to get some correlation between the flow regime and viscous losses in the oilfilm.

In addition to the above requirements, the test apparatus had to be as simple in design as possible, so that it could be built in a reasonable length of time and at an acceptable cost.

The basic apparatus was designed around a two inch diameter and one inch long bearing. Provision was made for using shorter bearings of the same diameter. The design and fabrication of basic components of the apparatus took approximately three months. After assembling the basic components, about six months were spent for preliminary testing and refining the apparatus and developing the necessary instrumentation.

Two series of tests were then carried out over a period of approximately three months. In the first series of tests, complete pressure distributions in the test bearing oilfilm were obtained operating at constant speed and load, but with different axial pressure gradients and datum pressures. In the second series of tests a transparent plastic bearing was used and cavitation phenomena were observed at constant speed and load, again operating with different axial pressure gradients and datum pressures. Cavitation phenomena were also recorded by still and motion picture photography.

Subsequent sections of this report contain detailed descriptions of the test apparatus and experimental procedures, presentation of experimental results, and conclusions based on experimental results. Experimental pressure distribution data are presented in graphical form, and in two cases a comparison is made with theoretical solution by Ocvirk (1). Cavitation phenomena in the oilfilm are shown by a number of photographs taken during the second test series.

II APPARATUS

Design Criteria

Since visual observation of the oilfilm behaviour was to be a basic part of the experimental investigation, the test bearing had to be made either of glass or some other transparent material. Transparent material being either very brittle or of low mechanical strength (e.g., plastics), a severe restriction was placed on the maximum pressure that would be allowable in the test bearing. In addition, provisions for instrument connections to pressure taps in a glass or plastic bearing placed additional stringent requirements on the apparatus design.

Due to these conditions it became evident that use of light lubricants in the test section would be the most practical approach for the following reasons:

1. Pressures developed in the oilfilm would be sufficiently low (even at high eccentricity ratios) so that excessive bearing distortion is unlikely.

2. Applied bearing loads and test section lubricant supply pressures (limited mainly by seals) would be within reasonable limits for application and measurement.

Preliminary calculations indicated that a journal bearing of two inch diameter and one inch length with radial clearance of the order of 0.002 in. would be practical. Using light lubricants (viscosities not exceeding 10 centipoise) and operating within speed range of 1000 to 5000

rpm, the maximum load that could be supported by such bearing would be about 100 lb. A load of this magnitude could be applied directly by means of weights, thus eliminating the need for more elaborate mechanical or hydraulic loading devices. Based upon the above considerations it was decided to use 100 lb. as the design load for the apparatus.

Other reasons for selecting the design speed range as 1000 to 5000 rpm were the following:

1. This range covers the speeds at which most journal bearings of the test bearing proportions are operating in practical applications.

2. Upper limit of 5000 rpm would permit the experimental investigation to be extended very close to, if not into, turbulent lubrication region which, according to Taylor's experiments,(5) starts at Reynolds number (Re) of approximately 2000. By going to lubricants with viscosities of the order of 0.5 centipoise (e.g., kerosene), Re values of the above magnitude could be achieved in the test bearing.

Arrangement of Apparatus

Several arrangements of the test bearing and journal were considered from such points of view as accuracy and ease of taking measurements, loading operation, visual observation, ease of exchanging bearings (in case of failures, or for changing dimensional configuration), fabrication problems, and costs. The arrangement of a vertical floating shaft supported by hydraulic pads, and stationary test bearing, was chosen as the most practical and simple one. Such an arrangement

automatically solved the alignment problems between the test shaft and electric motor drive and eliminated the need of correction for shaft weight and for friction losses in the driving mechanism. The stationary bearing, however, posed a problem of measuring the pressure distribution around the entire journal. This was solved by designing a loading assembly which allowed the applied load to be rotated around the stationary bearing, and thus to obtain pressure distribution measurements for a full 360^{o}.

Out of this basic configuration the apparatus evolved in its final form as illustrated in Figs. 1, 4, 5 and 6, shown in Appendix I, pp. 46 , 48, 49 and 50.

Test Apparatus Components

A cross-section of the apparatus is shown in Fig. 1, Appendix I, pg. 46, with the component parts being identified by numbers. In the description below these numbers will be given in brackets when various components are referred to.

1. The test section consists of a vertical 2 in. diameter, precision ground shaft [1] and one in. long bearing [6] (essentially one half of a bearing with central circumferential feed groove).

The vertical shaft is supported by two opposed, precision tapered roller bearings which in turn are housed in the floating disc assembly [3]. The preload on the bearings [20] is adjustable by a nut [2] to eliminate the play between the shaft and the floating disc assembly. This method of support provides good vertical alignment of the shaft (total runout less than 0.00005 in.), and at the same time it permits the shaft to take up

its equilibrium position within the rigidly supported test bearing. [6] As mentioned before, the vertical shaft eliminates the problem of compensating for the shaft weight as part of the applied load.

The test bearing is held rigidly between two rings [7] . These rings serve also as plenum chambers for lubricant circulation to and from the test section, house the lip seals isolating the plenum chambers, and act as manifolds for all pressure tap connections to the test section. The rings in turn are held between shouldered flanges [8] which keep the lip seals in place and affix the entire bearing assembly to the supporting bracket. [14]

The bearing proper is interchangeable so that clearance as well as ℓ/d ratio can be varied, and bearings made out of different materials can be used. The pressures in the film are picked up through two sets of pressure taps (three taps in each) 180 degrees apart. The pressure taps are connected through ports to the manifolds in the supporting rings [7] to facilitate the instrumentation piping and to keep the bearing proper uncluttered for better visual observation of the oilfilm. Manifolds in the supporting rings are designed to provide connections for up to four pressure taps in each set. To get complete pressure distribution in the circumferential direction, provision is made for rotating the applied load through an angle of 200 degrees.

2. The floating disc assembly [3] and motor support [18] tie the test shaft and the driving motor [19] into one unit so that alignment between the test shaft and the driving motor is maintained while the shaft is free to take up its equilibrium position in the bearing without any

friction forces present. On top of the floating disc assembly is a collar [13] and a slip ring [12] through which the load is applied to the test shaft. The pin in the sliding ring is for adjusting the load application point to coincide with the center of the test bearing, thus eliminating any external moment loads on the test section. Combining the driving motor and the test shaft into a single unit also allows one to measure the "net torque" on the test shaft since friction torques of the motor and supporting bearings are internal to the floating disc assembly. At the present time the floating disc assembly is kept from rotating by an arm resting against a stop on the underside of the loading sector [10] and no instrumentation is connected for taking torque readings. For taking torque readings the stop can be replaced by a spring scale or some other force measuring instrument. The torque readings would still include test bearing seal friction which could not be eliminated by design, (although it was tried) and would have to be corrected for.

3. The elimination of friction forces at the equilibrium position of the test shaft is accomplished by supporting the floating disc assembly between two hydraulic pads. The bottom pad [4] is fed through a circular groove supplied at two diametrically opposed points. Flow is radially inward and outward. Inward flow drains into a groove and is piped back to the reservoir; outward flow is collected by a plenum chamber, around the periphery of the disc, from which the top pad [5] is supplied. The flow in the top pad is radially inward and is drained through ports in the disc into the groove already mentioned. The amount of flow through

the top pad can be regulated by means of a bleed-off from the plenum for the top pad supply.

Since hydraulic pads separate the entire floating disc assembly from the rest of the apparatus, and the journal is also separated by the lubricant film from the test bearing, the existence of full hydrodynamic lubrication in the supporting pads (and in case of the test bearing made out of conducting material also in the bearing) is conveniently monitored by connecting a signal light in series with the floating disc assembly and the supporting pads. The separation of the floating disc assembly from the rest of the apparatus to make the circuit work is completed by insulating the load supporting wire and the dial gauges which ride directly on the test shaft.

During preliminary tests hydraulic pads were supplied with SAE 40 oil and strong vibrations of the floating disc assembly were excited, which made dial gauge readings impossible. However, this trouble was overcome by changing over to SAE 90 oil which apparently has adequate viscosity to damp out whirl and/or vibrations of the test shaft. Since the change-over to heavier oil no further troubles have been encountered and operation is sufficiently vibration-free so that the dial gauges can be read without difficulty.

4. The load is applied to the test shaft by weights hanging on the wire running over the pulley in the loading stand [11] and fastened to the pin in the sliding ring [12]. The loading stand can be moved in the groove of the sector [10] bolted to the underside of the hydraulic pad [4]. By positioning the loading stand and the sliding ring the direction of the

applied load can be varied through 200 degrees with respect to the pressure taps, thus giving complete circumferential pressure distribution around the journal with 20 degree overlap at changeover points from one set of pressure taps to the other.

5. The test section and the hydraulic pad assembly are rigidly supported by brackets [14] which were designed for bolting to existing collars [15] so as to utilize a drill stand [16] which was available. The drill stand is also used for supporting an instrument panel with pressure gauges and manifolds.

Auxiliary Equipment

The auxiliary equipment and instrumentation flow diagram is shown in Fig. 2., Appendix II, pg.47a. Three separate hydraulic circuits are used: lubricant supply to the test section, oil supply for hydraulic pads, and water supply for lubricant and roller bearing cooling.

1. The test section supply is by a vane pump from a lubricant reservoir equipped with a cooling coil to maintain constant lubricant temperature. The pump is of adequate capacity so that part of the discharge is bypassed back to the reservoir through a throttling valve which also serves as the primary supply pressure control for the test section.

The supply to the test section is passed through a ceramic filter to catch any particles that might damage the test bearing or the journal. Pressures in the supply and discharge plenums of the test bearing can

be further controlled by the valves in the bearing bypass and discharge lines. By manipulating the above three valves the pressures in both plenums can be selected to give desired axial gradient and datum pressure level in the test bearing. The test bearing bypass also provides for additional circulation through the plenums so that heat generated by seal friction is carried away and the test bearing temperature should be maintained within a few degrees of the lubricant supply temperature.

The supply reservoir was designed to be of small capacity (about 1/2 gal.) so that large quantities of lubricants would not be required in case it is decided to use special fluids (e.g., silicone compounds) for some tests.

2. Hydraulic pads are supplied from a larger (up to 5 gal.) reservoir by an eccentric gear pump. Again, primary pressure control is by means of a throttled bypass to the reservoir. Additional control is by a throttle valve in the supply line. The supply to the hydraulic pads is also passed through a ceramic filter to ensure clean supply, essential for proper pad operation (film thickness in hydraulic pads is approximately 0.002 in.). No cooling is provided for the oil used in the pads and this makes a periodic adjustment of the valves necessary during the first half hour of operation, until the apparatus attains its steady temperature.

3. Cooling of the roller bearings, particularly the lower one, is aided by a collar [21] around the lower portion of the floating disc assembly which is connected to the same water supply as the coil in the

lubricant reservoir. The cooling collar was added after preliminary tests indicated that the preload required to eliminate the play from the test shaft resulted in excessive heat generation and could have led to damage of the roller bearings. Preliminary test results indicated also that cooling of the roller bearings might need further improvement if the apparatus is going to be operated near the upper limit of the planned speed range.

4. Test shaft is driven by a vertical 3 HP, 3500 rpm 3-phase electric motor. A variable speed drive was initially planned for, but due to limitations of time and expense, it was decided to limit the present investigations to one speed.

5. To facilitate the alignment and changing of the test bearings, a small drum hoist was built into the instrument panel support collar so that the entire test bearing assembly can be easily slid up the column away from the test shaft.

Alignment of the Test Section

An angular frame of reference for measuring the relative positions of pressure taps with respect to the applied load direction was established by aligning the vertical axis of the test shaft [1] with that of the loading sector [10] as follows:

The hydraulic pad assembly [4] supporting the loading sector was first leveled by adjusting the column [16] and the bracket [15] . Next, reference marks located in the two mutually perpendicular planes passing through the sector axis and 0 degree and ±90 degree marks on the sector

respectively were established on the room floor by taking sights with the transit. Sights were then taken at a pointed cap placed over the end of the test shaft with the transit set up over the reference marks, and the test bearing assembly was shifted to make its axis coincide with the axis of the loading sector. After the alignment was checked out, reference marks were scribed onto the supporting column and collars, to be used for subsequent alignment purposes.

The pressure taps in the test bearing were aligned with ±90 degree marks on the loading sector by sighting at the vertical line scribed on the outside surface of the test bearing [6] and rotating the test bearing together with its supporting rings [7] to achieve the alignment.

Similarly the dial gauges were located in 0^{o} and $\pm 90^{o}$ planes of the loading sector by aligning the dial gauge plungers with the scribe lines on the pointed cap which in turn were sighted in by transit. The alignment was completed by adjusting the center at the back of the dial gauge to be on the transit hairline.

The axial alignment between the test shaft [1] and the bearing [6] was obtained by placing shims between the supporting collar and the bracket (adjustment in vertical 0^{o} plane of the loading sector) and by rotating the bracket about the central bushing around the big capscrew through the bracket [14] (adjustment in the vertical $\pm 90^{o}$ plane).

The parallelism of the journal and bearing axes is indicated by the maximum dial gauge readings for extreme positions of the journal within the bearing. A further check is provided by comparing dial gauge

readings with the diametral clearance obtained from bearing measurements prior to installation. However, the final check on the alignment was obtained by comparing the axial pressure gradients at the two opposed sets of pressure taps under static and dynamic no-load conditions. Symmetry of axial pressure gradients with stationary shaft indicates parallelism in the plane containing the pressure taps; and symmetry of axial pressure gradients with rotating shaft indicates parallelism in the plane normal to the plane above.

In the case of a transparent bearing with no pressure taps, the above method could not be used. In such instances a good check was obtained by observing the thickness variation of the oilfilm visually; and also by the symmetry of the bubbles formed in the film when the shaft was shifted from one extreme position to the other manually (without any lubricant feed to the plenum).

III INSTRUMENTATION AND MEASUREMENTS

Eccentricity

Eccentricity of the journal was measured by two dial gauges of the 0.0001 in./division accuracy riding directly on the top end of the test shaft. Dial gauges were located in the $+90^{\circ}$ and 0° planes of the loading sector, and were mounted on the supporting ring made out of insulating material to eliminate electrical contact between the test shaft and the rest of the test apparatus. The supporting ring was equipped with the adjustment screws for easier positioning of the dial gauges during the alignment procedure described in the previous section. In preliminary tests considerable chatter showed up in dial gauge plungers, resulting in excessive pointer fluctuations. To eliminate this chatter, nylon caps were installed over the plunger ends and a wick lubricator was provided for the shaft portion on which the dial gauge plungers were riding. This reduced dial gauge pointer vibration to within half a division, permitting gauge reading accuracy of the same order.

The zero setting of dial gauges was adjusted at the no-load condition and was checked out before each set of shaft displacement readings was taken. In each pressure distribution run displacement readings were taken with load at $+90^{\circ}$, 0° and -90° position of the loading sector, and checked out at the same stations at the end of the run.

In cavitation observations the displacement readings were taken only at one load position, namely at $+90^{\circ}$ because this load position

produced cavitation in the region best accessible for observation and photography.

Pressure Distribution

Instrumentation piping for pressure measurements in the test section is shown in Fig. 2, Appendix I, pg.47a together with the general piping diagram of the test apparatus.

Plenum pressures were measured directly with bourdon gauges connected to the supply plenum crossover line and to the discharge plenum return line.

Pressures in the test bearing oilfilm were measured by a pressure transducer energized from a 1000 cps constant voltage AC source, and a vacuumtube voltmeter (VTV). The electric circuit diagram is shown in Fig. 3, Appendix I, pg.47b. An oscilloscope connected to the VTV output was used as visual aid for monitoring the wave shape of the AC supply. The supply plenum pressure was used as reference pressure on the static side of the pressure transducer because this enabled one to monitor the supply pressure and reference pressure simultaneously by one bourdon gauge. The selection of pressure taps was accomplished by manifolds equipped with snap type valves for quick valving changes.

The bourdon gauges used in the experiment were calibrated against a dead weight tester, and the pressure transducer together with its electronic circuit was also calibrated with the dead weight tester connected to dynamic side, and reference pressure monitored by the previously calibrated bourdon gauge on the static side. The curves

established during the calibration procedure were used for all subsequent pressure data conversions. Calibration curve for the pressure transducer turned out to be nonlinear because instrumentation circuitry was balanced only capacitatively, inductive balancing being too difficult to achieve. For the same reason a perfect zero could not be obtained on the VTV scale and all readings were corrected for zero deviation.

Pressure distribution measurements were taken at 20^{o} angular intervals with pressure taps located at points 1/4 in., 1/2 in., and 3/4 in. from the supply plenum. A 20^{o} overlap in readings was taken at the changeover points from one set of pressure taps to the other to reduce the error due to inaccuracies in the bearing and the journal.

Rotation Speed

Rotation speed was measured by a "strobotac" at regular intervals, since with the induction motor drive the variations in speed were small, and continuous monitoring was not required.

Lubricant Temperature

Oil temperature was measured by a thermometer in the test section supply reservoir. No provisions for measuring temperatures in the test bearing oilfilm or plenums were included in the apparatus design since it was felt that lubricant flow would be sufficiently large to eliminate any significant temperature variations in the test bearing oilfilm.

Load

The applied load P was taken as equal to the weights hanging on the wire without any correction since in preliminary tests it was determined that under steady state conditions seals had virtually no spring effect that would tend to counteract the applied load.

Lubricant Viscosity

Viscosity of the diesel fuel used as lubricant during the tests was initially measured by a Brookfield Synchro-Electric Viscosimeter. The results were checked by an Ostwald viscosimeter and were found to be in error by a large factor; therefore viscosity readings obtained by the Brookfield Viscosimeter have been used only for comparison purposes of dyed, de-aerated and undyed diesel fuel. The data used for constructing the viscosity temperature graph in Fig. 10, Appendix II, pg. 56 are those obtained by Ostwald viscosimeter readings.

Torque

No torque measurements were made during the present investigation although provision for torque measurement was one of the requirements in the apparatus design.

IV EXPERIMENTAL DATA

Preliminary Tests

Preliminary tests were conducted using a bearing with a radial clearance of approximately 0.002 in., drilled for pressure taps and made out of lucite. The dimensional accuracy of this bearing was poor (out-of-roundness approximately 10% and taper up to 15% of the radial clearance). Also the pressure tap holes were too large (0.0625 in. dia.) causing excessive local disturbance in the oilfilm which in turn resulted in the early cavitation and had a strong localizing and stabilizing effect on the cavities, once these were established.

To obtain better accuracy it was decided to procure a glass bearing which would be dimensionally more stable and could be ground to closer tolerances. It was hoped that taper and out-of-roundness could be kept within 0.0001 in., which would keep the gap error within 5% for the radial clearance of 0.002 in. It turned out that a glass bearing ground to above tolerances could not be obtained locally, at least not in a reasonable time to complete the experimental investigation. The decision was then made to use a brass bearing for pressure distribution measurements, and a thick walled (3/4 in.) lucite bearing without pressure taps for observing the film behaviour visually. It was also attempted to machine a transparent bearing out of homolite CR-39 (a plastic about twice as strong as lucite), but this too proved to be dimensionally unstable, probably because of the laminated construction which had to be used since only 1/2 in. thick material was available.

Pressure Distribution Measurements

In the first series of tests the 2.0000 in. O.D. shaft was used in combination with a brass bearing of 2.0041 in. average I.D. (for detailed I.D. measurements, see Table I in Appendix II, pg. 51) and one inch long. The bearing was drilled for six 0.020 in. dia. pressure taps located in two sets 180° apart, each set having pressure taps at one quarter, half and three quarters of the axial extent of this bearing.

Diesel fuel was used as lubricant because it had viscosity of the right order and because it was inexpensive and readily available. Before starting the test series, diesel fuel in the supply reservoir was deaerated under vacuum for about 12 hours to remove dissolved air so that cavitation in the low pressure region would not occur until actual vapor pressure of the lubricant was reached.

The test series consisted of five runs with 30 lb. applied load and one run with 60 lb. applied load. The first four runs were intended for investigating the pressure distributions under different axial pressure gradients; for this purpose supply pressures of 10, 15, 20 and 30 psig. were used with discharge at 0 psig. The fifth run was made with 16 psig. supply and 15 psig. discharge pressure to obtain the pressure distribution under elevated datum pressure but with low axial gradient. The run with 60 lb. load, 25 psig. supply and 19.25 psig. discharge pressure was made to obtain the pressure distribution data at a higher eccentricity ratio.

With the induction motor drive it was not possible to make all runs at exactly the same speed; however, the difference of speed was relatively small, the highest speed run being at 3510 and the lowest at

3470 rpm. The speed variation during any one run did not exceed 15 rpm.

Experimentally obtained pressure distribution data are shown graphically in Fig.'s 7 to 12, Appendix II, pp. 53 to 58, together with variables for each run and the experimental values of eccentricity ratio n and attitude angle Φ. The values of n and Φ stated on the graphs are average values obtained by averaging experimental readings, with load at $+90^{\circ}$ and -90° of the loading sector, and this result in turn with the readings with load at 0°, to reduce errors resulting from circumferential variations in the journal and bearing. The value of radial clearance C_R used in calculating n is 0.00205 in. or one half of the average diametral clearance based on the I.D. measurements of the bearing. This value of C_R was consistent with the extreme dial gauge readings for test bearing after it was installed in the apparatus.

Viscosity values stated on graphs correspond to the diesel fuel temperatures measured in the supply reservoir (no other temperature measurements were taken) and do not represent the exact viscosity values in the test bearing oil film.

In Fig.'s 10 and 11, showing pressure distributions for the test runs with 30-0 psig. and 16-15 psig. supply and discharge pressures respectively, theoretical pressure distributions as calculated on the basis of Ocvirk's solution (1) are also shown in dotted lines for comparison.

Observation and Photography of Cavitation

For the second series of tests, the 2.0000 inch O.D. shaft was

used in combination with a lucite bearing of 2.0034 inch average I.D. (for detailed measurements see Table I in Appendix II, pg. 51) and one inch long, without any pressure taps. The series consisted of some 26 runs, all with 60 lb. applied load, but with various axial gradients and datum pressures. Cavitation phenomena were successfully recorded by still photography in nine runs and by motion picture photography in five runs.

In the first few trial runs during which cavitation was observed visually, it became evident that diesel fuel was too light-colored and did not give adequate contrast even for good visual observation, not speaking of photography. Addition of red gasoline die was tried which produced a marked increase in contrast. In fact, the contrast was so much improved that successful photography of cavitation phenomena began to appear feasible.

The first set of photographs turned out poorly, indicating that sufficient contrast between the cavitation and the continuous film region was still lacking. To increase the contrast further a green filter was procured which would absorb red light and make the continuous oilfilm region look darker. The second set of photographs showed up cavitation to some extent, but results were still far from satisfactory. The main difficulty was created by floodlight reflections on the shaft which produced bright spots on the shaft, and resulted in overexposed areas on the negatives where all contrast was blanked out. To eliminate these troublesome reflections, a mat white cylindrical screen was placed around the test section and four spotlights were directed downwards on

the screen from above, so that the test bearing was illuminated by indirect light only. Photography and observation were carried out through peepholes cut into the screen.

After trial exposures indicated that lighting was adequate and free from bright reflections, a series of photographs were taken of the cavitation phenomena in the bearing oilfilm. Six runs were made with supply pressures from 4.3 to 10 psig. and 0 psig. discharge in order to record cavitation phenomena with increasing axial gradient. Three additional runs, with supply pressures from 11.8 to 14.3 psig. and discharge pressures from 8.6 to 10 psig. were made to record cavitation phenomena with low axial gradient but at elevated plenum pressures.

Photographs of these test runs are shown in Figs. 13-22, Appendix II, pp. 59 to 63 , together with operational parameters and experimental eccentricity ratio n and attitude angle ϕ for each run. In this case the average radial clearance C_R based on the I.D. measurements of the lucite bearing did not agree with the value obtained by extreme dial gauge readings on the installed test bearing. The C_R value was checked by dial gauges several times after the apparatus warm-up period and during the test runs and was found to be consistently 0.0014 inches allowing for ±0.00005 inch dial gauge reading accuracy. This value was considered to be more correct, since it was likely that the lucite bearing underwent some deformation due to imposed axial stress and temperature change. Approximate extent and behaviour of the cavity are also stated for each case. The angular coordinate system

used is the same as for the pressure distribution graphs, i.e., zero degrees at the applied load, increasing in the direction of rotation. In all photographs the location of the camera is at station 180°; rotation is from right to left, with the closest approach point at the extreme right of the photographs. The supply plenum is at the top so that applied gradient and flow are directed downward.

The experimental values of n and Φ are based on readings with load at one station only, since the screen placed around the test section prevented rotation of the load. Hence, values of n and Φ stated under each photograph are in all probability less accurate than those obtained in connection with the pressure distribution measurements where readings from three stations were averaged to obtain final values of n and Φ.

To provide an additional permanent record of the cavitation phenomenon and particularly of its unstable nature at high axial gradients and/or datum pressures, motion pictures were taken of five additional runs. Three of these runs were made with increasing axial gradient and two with small axial gradient at elevated datum pressures.

V DISCUSSION OF EXPERIMENTAL RESULTS

Pressure Distribution with Elevated Datum Pressure

The pressure distribution obtained in the test run where cavitation was suppressed by the elevated plenum pressures while the axial gradient was kept at a minimum (1 psi) is shown in Fig. 11, Appendix II, pg. 57 . The pressure readings give continuous curves indicating absence of cavitation. Small discontinuities aside from random scatter of experimental points occur only at the changeover points from one set of pressure taps to the other. These are consistent for high as well as for low pressure regions and are caused by circumferential variations of the journal and the test bearing. The axial pressure distribution is very nearly symmetric, as would be expected on the basis of the theoretical solutions.

Since cavitation apparently does not exist in this case, it would be of interest to compare the experimental pressure distribution with that of Ocvirk's solution (1). Applying appropriate boundary conditions to Ocvirk's solution, we get the following expression for the pressure distribution in the journal bearing oil film

$$P = \frac{3\mu U}{r C_R^2}\left(\ell z - z^2\right)\frac{n \sin\theta}{(1+n\cos\theta)^3} - (P_s - P_D)\frac{z}{\ell} + P_s \qquad (1)^*$$

Integrating this pressure distribution around the entire bearing gives the

---

* For a detailed derivation of Eqs. 1, 2, 3 see Appendix III, pp. 69-71.

total load components as

$$P_x = 0 \tag{2}$$

and

$$P_Y = P = \frac{\mu U \ell^3}{2 C_R^2} \frac{n\pi}{(1-n^2)^{3/2}} \tag{3}$$

resulting in the attitude angle

$$\phi = \tan^{-1} \frac{P_Y}{P_x} = \tan^{-1} \infty = 90^\circ$$

Since the actual value of viscosity μ in the oilfilm could not be determined experimentally (oilfilm temperature was not measured) the value of μ was calculated on the basis of Eq. 3 using the experimental values for eccentricity ratio, applied load and rotation speed. The value of μ thus obtained was then used in Eq. 1 to construct theoretical pressure distribution curves shown by dotted lines in Fig. 11.

As a check, comparison of the calculated value of μ = 3.71 centipoise with the viscosity-temperature curve in Fig. 24, Appendix II, pg. 65 , gives the corresponding oilfilm temperature as 94°F. Thus the oilfilm temperature in the journal was 19°F higher than measured at the supply reservoir, which certainly is of the right order of magnitude.

As can be seen, the agreement between theoretical and experimental curves is as good as could be expected, considering all the experimental errors involved. The largest deviation is in the extreme

high and low pressure regions amounting to about 1.5 psi or less than 4% of the maximum circumferential pressure variation given by theoretical solution for the middle line ($\ell/2$) of the bearing. Agreement with theory is also very good for the attitude angle Φ and for the angular location of the extreme high and low pressure regions.

The pressure distribution curves based on the test run with 60 lb. applied load shown in Fig. 12, Appendix II, pg. 58 , are essentially of similar general shape with the exception that larger pressure differences are developed in the oilfilm as the result of higher eccentricity ratio n. The cavitation is effectively suppressed by elevated datum pressure and imposed axial pressure gradient as indicated by good continuity of experimental points, except for a small region near the discharge plenum. The small discontinuities at the pressure tap change-over points are consistent with other test runs, indicating that this error is inherent in the bearing and journal.

Pressure Distribution with Axial Gradient

The effect of increasing axial gradient on the pressure distribution in the journal bearing oilfilm can be seen in Figs. 7 to 10, Appendix II, pp. 53 to 56, showing experimental pressure distributions with 10, 15, 20 and 30 psi/in. axial pressure gradient and 30 lb. applied load.

Plots of the experimental data show that the circumferential pressure distribution at any one station ($\ell/4$, $\ell/2$ and $3\ell/4$) is relatively unaffected by axial gradient. Allowing for experimental errors, the corresponding curves are all of approximately the same shape. The effect of increasing axial gradient is merely to separate the curves to

different "datum" pressure levels. Small differences between corresponding curves are probably due to experimental errors. However, there is a slight but consistent tendency for corresponding curves to become more peaked as the axial pressure gradient increases. This effect is probably due to the differences in the flow patterns resulting from the suppression of reverse axial flow by imposed axial pressure gradient. As can be seen in Fig. 7, the high pressure region at all three pressure taps exceeds the supply pressure; consequently there is a large region where reverse axial flow takes place and part of the oil is forced back into the supply plenum. On the other hand, Fig. 10 indicates that when operating with a high imposed axial pressure gradient the reverse pressure gradient is almost entirely overcome, and therefore axial flow should be unidirectional with the exception of a small region. The implication is, that for an axial pressure gradient where axial flow reversal takes place in the high pressure region the peak pressures tend to be reduced, while for sufficiently high axial pressure gradient the reverse flow is suppressed and pressure distribution curves tend towards more peaked form.

Also, it is of interest to note that with a low axial pressure gradient, extreme high and low pressure regions occur at or very near the midpoint ($\ell/2$) of the bearing while with a high axial pressure gradient these extreme pressure regions are moved axially apart; the high pressure region moves closer to the feed groove and the low pressure region moves closer to the discharge end of the bearing. Thus by in-

creasing the axial pressure gradient it is possible to force the region of cavitation towards the outer edge of the bearing with the central supply groove, and for all practical purposes suppress it entirely. In Figs. 7 to 9 the cavitation region as indicated by dotted portions of the curves is decreasing with the increasing axial pressure gradient, until in Fig. 10 it disappears completely.

Since the extent of the cavity and the pressure within the cavity is not exactly determined, the comparison of the experimental pressure distribution, as well as the eccentricity ratio and the attitude angle is meaningful only for the case where no cavitation exists, and thus complete pressure distribution can be measured. In Fig. 10, the theoretical pressure distribution based on Eq. 1 with the appropriate boundary conditions is shown by dotted lines for comparison. Again the viscosity value used in Eq. 1 is calculated by making use of Eq. 3 and the experimental data. As can be seen from Fig. 10 the agreement between theoretical and experimental pressure distribution curves is considerably poorer when the bearing is operated with a high axial pressure gradient. The biggest deviation is in the peak high pressure region where at the midpoint of the bearing the difference is 3.0 psi or 10% of the maximum circumferential pressure variation predicted by theory. The error is even higher at 3/4 axial distance from the supply plenum where respective values come out to be 4.6 psi or 16.7%. It would be interesting to know whether this disagreement is due to reversals in axial flow direction in the high pressure region as discussed above or

to some other phenomena. The experimental data are insufficient for drawing any conclusions. One or two additional experimental pressure distribution graphs taken, say, with 25 psi/in. and 35 psi/in. axial pressure gradient would be very valuable at this stage for comparison purposes. Such experimental graphs should provide a clear indication as to whether the disagreement is increasing or decreasing with the increasing axial pressure gradient. If an increased axial pressure gradient will produce better agreement, then indication is that reversals of the axial flow direction could account for deviations; in case the opposite proves to be true, some different explanation must be sought. The results with a minimum axial pressure gradient operation, where flow is unidirectional (outward) in the high pressure region, show that in cases where no axial flow reversals take place, the agreement with Ocvirk's theory is good.

Further pressure distribution measurements with sufficiently high axial gradients so that cavitation would be suppressed, should yield more useful information as to the causes of this disagreement with theory.

The experimental attitude angle and angular locations of the extreme pressure regions are still in very good agreement with the theory.

Visual Observation of Cavitation

As stated previously, cavitation in the journal bearing oilfilm was observed in some 26 runs. Basically there were two types of conditions at which cavitation was observed. Operating with a high axial pressure gradient and atmospheric discharge, typical behaviour and the effect of

progressively higher axial pressure gradient are shown in Figs. 13 to 19, Appendix II, pp. 59 to 62. Operating with a low axial gradient and at elevated plenum pressures, typical behaviour and the effect of progressively higher plenum pressures are shown in Figs. 20 to 22. Appendix II, pp. 62 and 63. To further illustrate unstable cavitation behaviour enlarged strips of motion picture record are also shown in Figs. 23 to 25, Appendix II, pp. 64 to 66.

At a low axial pressure gradient the cavity is very well defined and stable in its shape Fig. 13, but contrary to the assumption that it extends over 180°, i.e., theoretical negative pressure region, the extent of the cavity is about 260° circumferentially. Also the cavity covers about two thirds of the bearing length at the start and narrows down to about half the bearing length before collapsing. The narrowing down takes place at the upper edge where positive supply pressure is applied. This clearly indicates that the extent of the cavitation region at low axial pressure gradient is much larger than expected on the basis of the theoretical pressure distribution. The "effective" high pressure region that supports the load covers only some 100°, a little more than one quarter of the circumference. The eccentricity ratio is relatively high, and attitude angle tends toward the value predicted by Ocvirk's theory, mainly because angular orientation of the high pressure region agrees well with theory as was already pointed out by the experimental pressure distribution.

The separation of the cavity into strips as seen in Figs. 13, 14 and 23, indicates that even minute bearing surface irregularities have a strong influence on the initiation and location of the cavity (this was also

observed in preliminary tests where strong local disturbance was created by pressure taps).

As the axial pressure gradient is increased, Fig. 14, the cavity is narrowed down from the supply side while the discharge side is unaffected. The angular extent is also reduced, and the leading edge where the cavities are initiated shows first signs of instability. There is no apparent change in the eccentricity or the attitude angle.

Further increase in the axial pressure gradient, Fig. 15, produces instability at the top edge of the cavity and narrows it down even more, particularly at the tail end of the cavity. There is increased instability at the leading edge, the eccentricity ratio n drops (although there is little change in the angular extent of the cavity) and the attitude angle increases. At 8.8 psi/in. axial pressure gradient, first signs of marginal stability appear for the cavity. The only boundary that remains stable and well defined is the one on the discharge side. The leading edge with the exception of the lower corner is subject to great fluctuations, producing also variations in the tail end of the cavity. Figs. 16 and 17 are taken at two different times and show the appearance and collapse of the cavity at the leading edge. This typical unstable behaviour can best be observed in the motion picture record of cavitation (see Figs. 23 to 25). The angular extent and width of the cavity are both markedly reduced which also shows up in the reduced eccentricity ratio. The attitude angle seems to be affected very little.

Figs. 18 and 19 show cavitation in two different runs where the axial pressure gradient is the same (10 psi/in.), although the speed is slightly

different. In both cases the cavity was highly unstable and took different shapes for a fraction of a second; two of these typical shapes appear on the photographs. Also, at the above axial pressure gradient, first instability appeared at the bottom edge of the cavity and the entire cavity tended to jump axially back and forth over the third quarter of the bearing. The strong localizing influence of an invisible surface irregularity is again apparent in Fig. 19. It is of interest that attitude angle becomes larger than 90° as the angular extent of the cavity approaches half the circumference of the bearing. This behaviour is in good agreement with attitude angles obtained during pressure distribution measurements with limited cavitation.

For axial pressure gradients larger than 10 psi/in., the cavity could not be decreased any further. The cavity became so unstable that it appeared only for a fraction of a second, and successful photographic recording became almost impossible. This completely unstable stage of cavitation can be observed in the motion picture record of the oilfilm behaviour (see Fig. 24). With an axial pressure gradient sufficiently high to result in unstable cavitation behaviour the effects that even small surface irregularities (e.g., pressure tap) can produce become very pronounced. In the smooth plastic bearing it was virtually impossible to produce any stable cavitation with relatively low axial pressure gradient (limiting value was about 10 psi/in.), while in the brass bearing much smaller and well localized cavities were stable at considerably higher axial pressure gradients (and lower eccentricity ratios).

Such strong effect of bearing surface defects on the cavitation also implies that pressure distribution measurements in the low pressure regions are not truly representative of the conditions in the smooth bearing because the very presence of pressure taps influences the oil film behaviour in the low pressure region. This error is of course eliminated when cavitation is suppressed by a high axial gradient or elevated plenum pressures.

Similar behaviour was indicated by cavitation observed in preliminary tests with a plastic bearing drilled for pressure taps, but as pointed out, these pressure taps were too large and the bearing itself was of poor dimensional accuracy for drawing any conclusions. It would be of real interest to make pressure distribution measurements with a dimensionally stable glass bearing equipped with pressure taps and then compare cavitation patterns with those in a smooth bearing of identical dimensions, if such bearings could be procured.

With a low axial pressure gradient but elevated plenum pressures, cavities are localized axially near the middle of the bearing as can be seen in Figs. 20 and 21. Also the cavities are somewhat more stable, and considerably smaller marginally stable cavities can be observed (e.g., Fig. 20, where cavity width is about one fourth of the bearing width and angular extent some 130^{o}). Here too, unstable behaviour begins at the leading edge where the cavity is initiated. Of particular interest is the unstable cavitation shown in Figs. 21 and 22. In Fig. 22 the tail end does not collapse uniformly as in all other cases with larger size cavities; instead the cavity narrows down and breaks up into separate

bubbles which tend to penetrate into the high pressure region before they collapse. This becomes even more pronounced at the conditions of Fig. 22 test run. In this case small bubbles occasionally fail to collapse even in the high pressure region and are carried right around into the low pressure region where they initiate a new cavity. The path of such a bubble is faintly visible at about three quarter axial distance in the region corresponding to closest approach (i.e., extreme right). A similar bubble path is even more clearly visible in the second and third frames of Fig. 24, under slightly different operating conditions. A further study of this phenomenon could provide important information for explaining fatigue failures of bearing surfaces.

One additional phenomenon of interest was observed in the tail end region of large cavities, the region not visible on the photographs. At the point where the cavity collapsed, small droplets of lubricant tended to separate and were drawn into the cavity where they slowly drifted in the direction opposite to the journal rotation, indicating that there is a pressure gradient within the cavity in the direction opposite to rotation.

Sources of Error

Maximum instrumentation errors as based on manufacturer's data follow:

1. Pressure transducer non-linearity and hysteresis up to ± 0.5% of full scale excursion.
2. Vacuum tube voltmeter error up to ± 2% of full scale excursion.
3. Constant voltage supply voltmeter error up to ±1% of full scale excursion.

Theoretically, these errors could add up to a substantial percentage value, but even if they do, the experimental pressure data would be affected only by the amount of variation in the total error, since the entire instrumentation circuit was calibrated as a unit using a calibrated pressure gauge and a deadweight tester. All non-linearities and other inherent errors were thus accounted for by using the instrumentation calibration curve for converting the experimental data. Since there was very little variation in the conditions from one run to the other, it is reasonable to assume that variations in the total instrumentation error that do affect the experimental data are negligible as compared to other experimental errors that are discussed below.

Errors that cannot be corrected for are the actual reading errors of instruments and fluctuations in the reference pressure and the pressure transducer excitation voltage.

The reference pressure was maintained constant throughout each run within 0.1 psi, resulting in a relative error of not more than 0.4% with respect to maximum pressure variation when operating with 30 lb. applied load. The pressure transducer excitation voltage was maintained constant within 0.05 V during each run, resulting in a maximum error of approximately 0.5% with respect to the excitation voltage of 9.7 V used throughout the experiments. The reading accuracy of the VTV can be estimated to be within 1% of the full scale deflection. Thus, total estimated random error in the experimental readings is of the order of ±2% of the maximum pressure variation of some 35 psi when operating with 30 lb. applied load. This amounts to about ±0.7 psi, which is con-

sistent with the scatter of the experimental points in the graphs. Errors are somewhat larger in the low pressure regions because it took a relatively long time to attain equilibrium pressures in the instrumentation piping, and even though considerable care was taken in obtaining low pressure readings, it is likely that some readings are not exactly at equilibrium conditions. Of course, with cavitation present, pressure readings become meaningless and serve merely as an indication of discontinuity, thereby giving an indication of the extent of the cavitation region.

The largest experimental errors in pressure distribution measurements are resulting from taper and out-of-roundness of test bearings. As can be seen from the measurements in Tables I and II, Appendix II, pp. 51 and 52 , the taper and/or out-of-roundness result in approximately 5% and 6% variation in C_R value for brass and lucite bearings respectively. If C_R variation in lucite bearing is estimated on the basis of the C_R value used for calculating n, then error can be as high as 7.1%. It is impossible to make any corrections for these errors since no instruments other than standard micrometers were available for I.D. measurements; thus the nature of diametral variations could not be established. It could be that the effects of diametral variations are more pronounced when operating with high axial pressure gradient; however, even this consideration would not provide a satisfactory explanation for the large differences (up to 16.7% deviation) between the theoretical and the experimental pressure distribution as observed with high axial pressure gradient.

As mentioned previously, the dial gauge reading accuracy was within half a division, or 0.00005 in. Thus, in the vicinity of 90 degree attitude angle, the maximum resulting error in ϕ for a single reading is of the order of 3.5 degrees (average second dial gauge reading is taken as 0.00075 in.). For experimental values of ϕ stated on the pressure distribution graphs, this error should be reduced to a negligible amount since essentially an "average" of six readings at three different stations was used in calculations. Also, for ϕ values stated with photographs, error should, in general, be considerably less, since each set of readings was checked for consistency at the end of the run.

VI CONCLUSIONS

Experimental results show that circumferential pressure distribution curves are of modified sinusoidal shape, having a positive and a negative pressure region with respect to the datum pressure.* With a small axial pressure gradient and low supply pressure the datum pressure may be sufficiently low so that extreme negative pressures fall below the vapor-pressure level of the lubricant. In such cases a negative pressure region has a tendency to be relieved as evidenced by discontinuities in the experimental pressure distribution curves. Visual observations of the oilfilm behaviour have shown conclusively that the mechanism by which negative pressures are relieved is cavitation, and not reverse flow in the divergent oilfilm as suggested by Wannier's solution (4). Apparently, clearances in journal bearings are so small that Wannier's solution is not applicable.

Agreement between experimental results and Ocvirk's short bearing solution (1) was found to be very close when operating with low axial pressure gradient but at sufficiently high "datum" pressure so that cavitation was completely suppressed. On the other hand, when operating with high axial pressure gradient (cavitation again completely suppressed) considerable differences between experimental and theoretical pressure distributions were found, while for attitude angle the agreement was still very close. At lower axial gradients and/or datum pressures where cavitation was present, no comparison was attempted since visual observations of oilfilm behaviour indicated that Ocvirk's assumption about the entire load being supported by positive pressure region is not valid under

*Datum pressure is defined as the line of symmetry for a particular circumferential pressure distribution curve.

actual operating conditions. Thus for engineering applications Ocvirk's solution appears to be quite accurate where short journal bearings are operated at elevated "datum" pressure and low axial pressure gradient (e.g., submerged and pressurized bearings). For more common applications where cavitation might be partly or fully suppressed by high axial pressure gradient only, Ocvirk's solution appears to be inadequate unless it can be corrected to account for the effect that high axial pressure gradient has on the pressure distribution. In cases where cavitation is only partly suppressed, additional complications arise, since the extent of the cavity is rather difficult to determine. Eccentricity measurements made during visual observation of oilfilm behaviour showed that eccentricity ratio and attitude angle are dependent on the extent of cavity in the oilfilm. Thus it becomes necessary to determine the extent of cavitation region on the theoretical basis in order to predict the eccentricity ratio, i.e., the minimum oilfilm thickness for a given load. A conservative estimate of the total load that a bearing is capable of supporting can still be made by using Ocvirk's assumption, but a close engineering design cannot be achieved unless a better model of the actual oilfilm can be constructed.

Visual observation also showed that even though cavitation was primarily governed by "datum" pressure and/or axial pressure gradient, the shape and location of the cavity was strongly influenced by the defects and roughness of the bearing and journal surfaces. Operating conditions resulting in marginally stable or unstable cavitation are most interesting from a practical application viewpoint. It was observed that under these

conditions, the tail end of the cavity tended to separate into small bubbles which were carried into and occasionally through the high pressure region. This phenomenon may have considerable significance in connection with fatigue failures observed in many journal bearings, and a more detailed investigation in this particular area could provide some very useful information.

VII REFERENCES

1. Dubois, G. B., and Ocvirk, F. W., Analytical Derivation and Experimental Evaluation of Short-Bearing Approximation for Full Journal Bearings, NACA 1157, 1953.

2. McKee, S. A., and McKee, T. R., Pressure Distribution in Oil Films of Journal Bearings, Trans. ASME, RP-54-8, Vol. 54, 1932, pp. 149-165.

3. Cole, J. A., Low Pressure Regions Occurring in the Hydrodynamic Films of Journal Bearings. Scientific Lubrication, vol. 3, 1951, p. 10.

4. Wannier, G., A Contribution to the Hydrodynamics of Lubrication, Quarterly of Applied Mathematics, vol. 8, 1950, pp. 1-32.

5. Cameron, A., and Wood, W.L., The Full Journal Bearing. Proceedings of Inst. of Mech. Engineering, vol. 161, 1949, pp. 59-64.

6. Wilcock, D.F., Turbulence in High-Speed Journal Bearings. ASME Transactions, vol. 72, 1950, pp. 825-834.

7. Jacobson, M.J., Charnes, A., Saibel, E., The Complete Journal Bearing with Circumferential Oil Inlet. ASME Transactions, vol. 77, 1955, pp. 1179-1183.

8. McKee, S.A., White, H.S., Oil Holes and Grooves in Plain Journal Bearings. ASME Transactions, vol. 72, 1950, pp. 1025-1034.

9. McKee, S.A., Oil Flow in Plain Journal Bearings. ASME Transactions, vol. 74, 1952, pp. 841-848.

10. Wilcock, D.F., Rosenblatt, M., Oil Flow, Key Factor in Sleeve-Bearing Performance. ASME Transactions, vol. 74, 1952, pp. 849-866.

11. Kreisle, L.F., Very Short Journal-Bearing Hydrodynamic Performance Under Conditions Approaching Marginal Lubrication. ASME Transactions, vol. 78, 1956, pp. 955-963.

12. Dawson, D., Investigation of Cavitation in Lubricating Films Supporting Small Loads. IME Conference on Lubrication and Wear. Paper No. 49, Oct. 1957.

13. Swift, H. W., The Stability of Lubricating Films in Journal Bearings. Proceedings, Institute of Civil Engineers, London, vol. 223, part I, 1931-32, pp. 267-288.

14. Gross, W. A., Film Lubrication V. Infinitely Long Incompressible Lubricating Films of Various Shapes.

15. Cole, J. A., and Huges, C. J., Visual Study of Film Extent in Dynamically Loaded Complete Journal Bearings. IME Conference on Lubrication and Wear. Paper No. 87, Oct. 1957.

APPENDIX I: ILLUSTRATION OF APPARATUS AND INSTRUMENTATION.

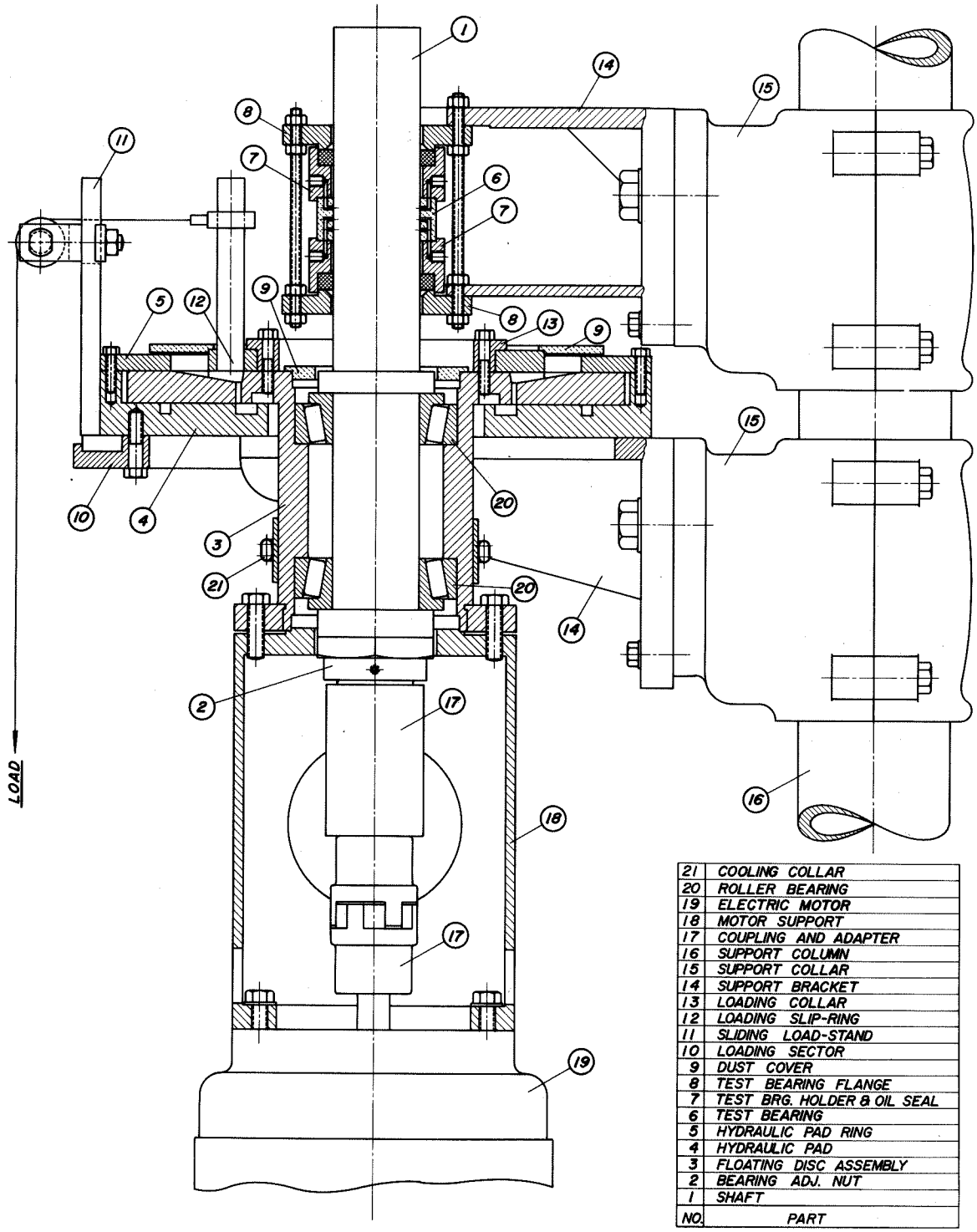

NO.	PART
21	COOLING COLLAR
20	ROLLER BEARING
19	ELECTRIC MOTOR
18	MOTOR SUPPORT
17	COUPLING AND ADAPTER
16	SUPPORT COLUMN
15	SUPPORT COLLAR
14	SUPPORT BRACKET
13	LOADING COLLAR
12	LOADING SLIP-RING
11	SLIDING LOAD-STAND
10	LOADING SECTOR
9	DUST COVER
8	TEST BEARING FLANGE
7	TEST BRG. HOLDER & OIL SEAL
6	TEST BEARING
5	HYDRAULIC PAD RING
4	HYDRAULIC PAD
3	FLOATING DISC ASSEMBLY
2	BEARING ADJ. NUT
1	SHAFT

FIG. I.

SECTION OF TEST APPARATUS

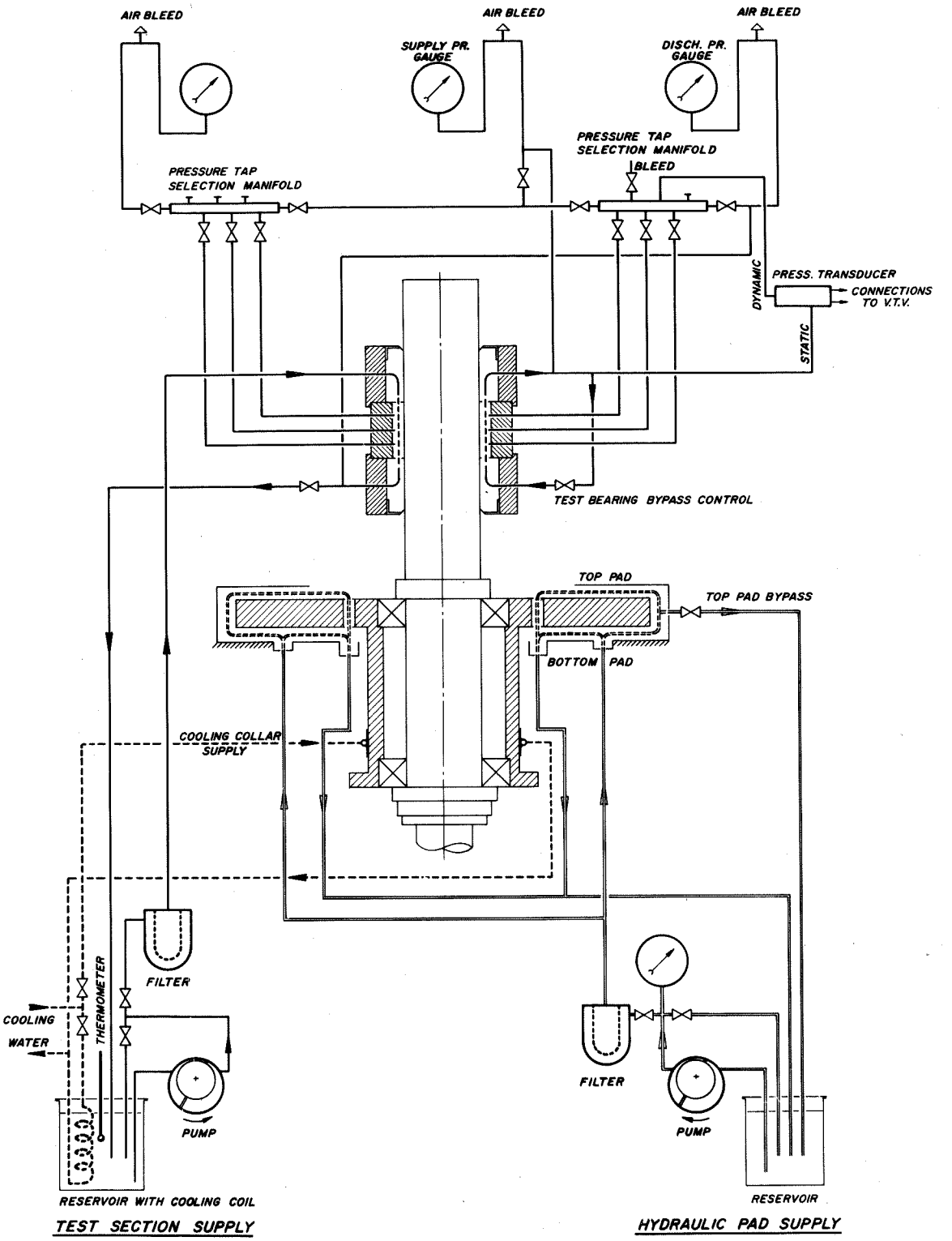

FIG. 2.

INSTRUMENTATION AND SERVICE PIPING DIAG.

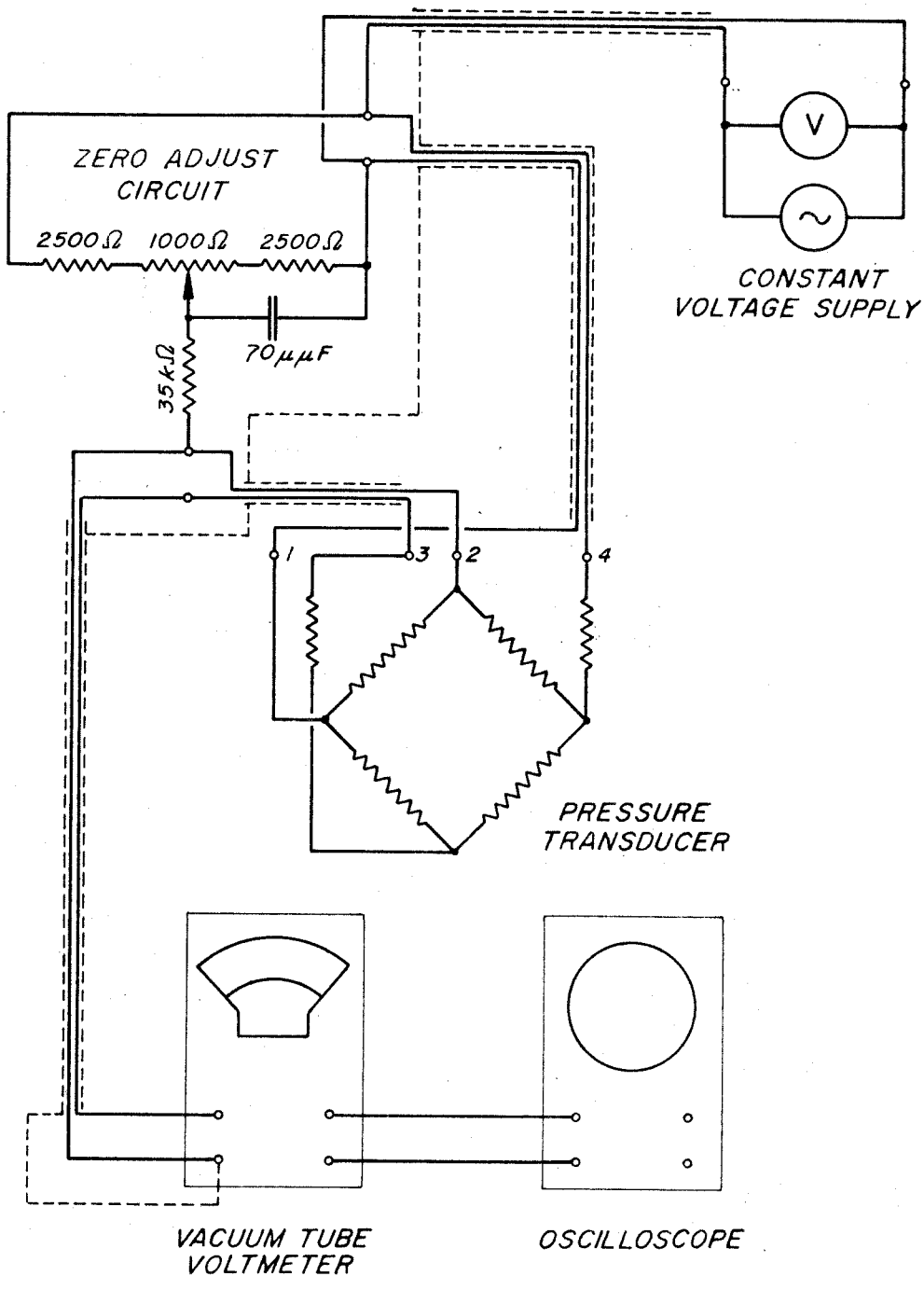

FIG. 3.

PRESSURE TRANSDUCER INSTRUMENTATION

CIRCUIT DIAGRAM

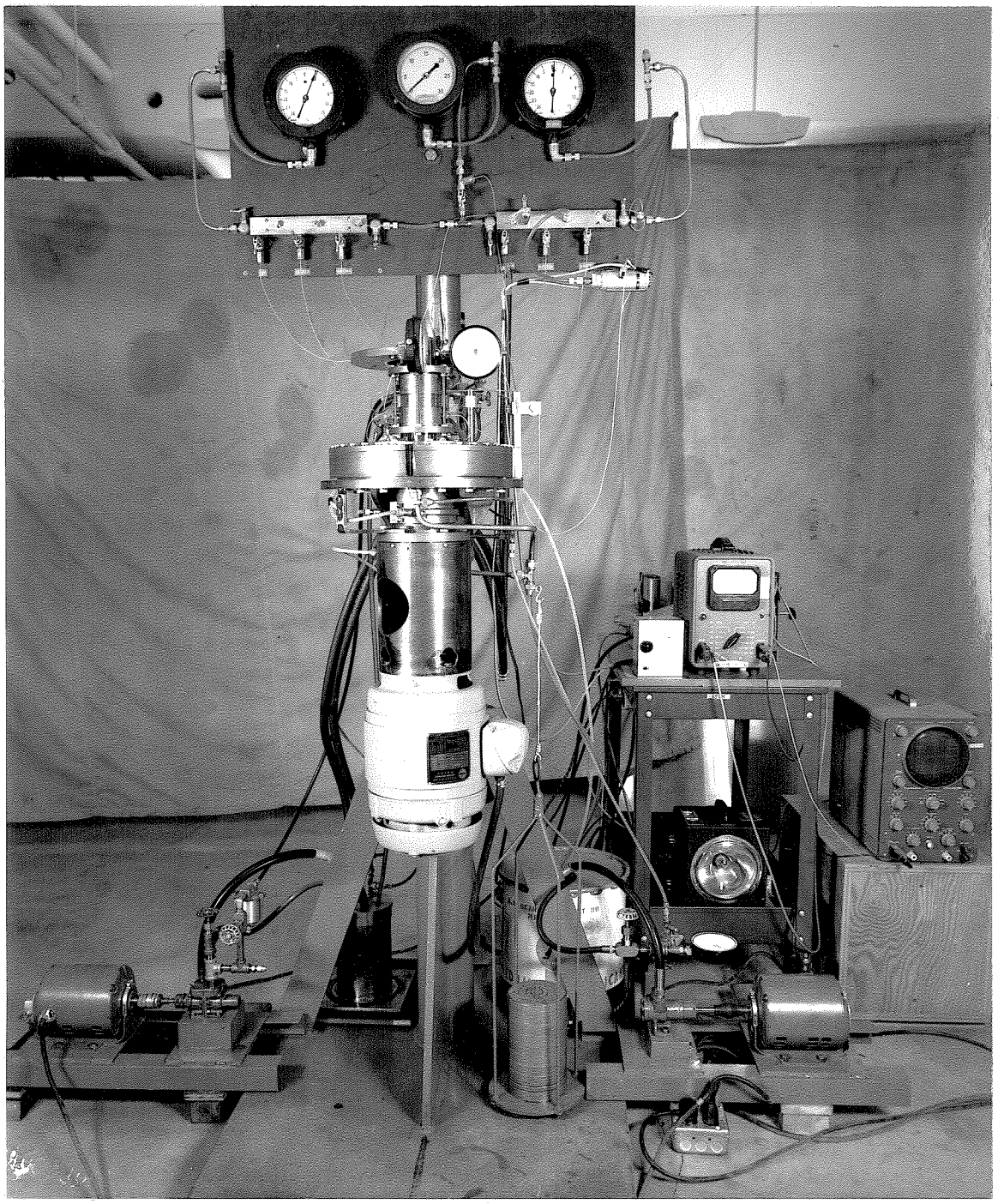

FIG. 4

FRONT VIEW OF APPARATUS AND AUXILIARY EQUIPMENT.

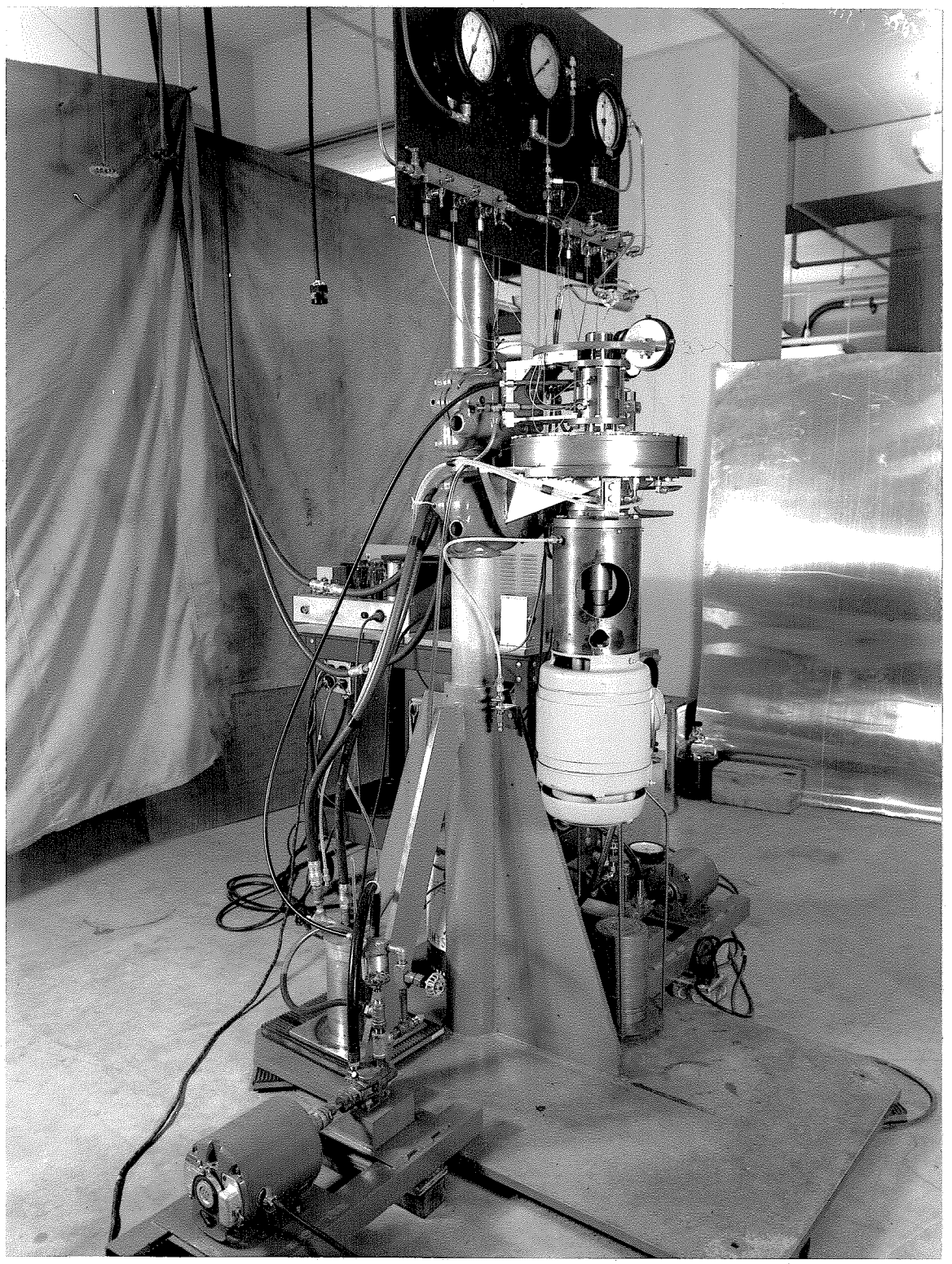

FIG. 5

SIDE VIEW OF APPARATUS AND AUXILIARY EQUIPMENT.

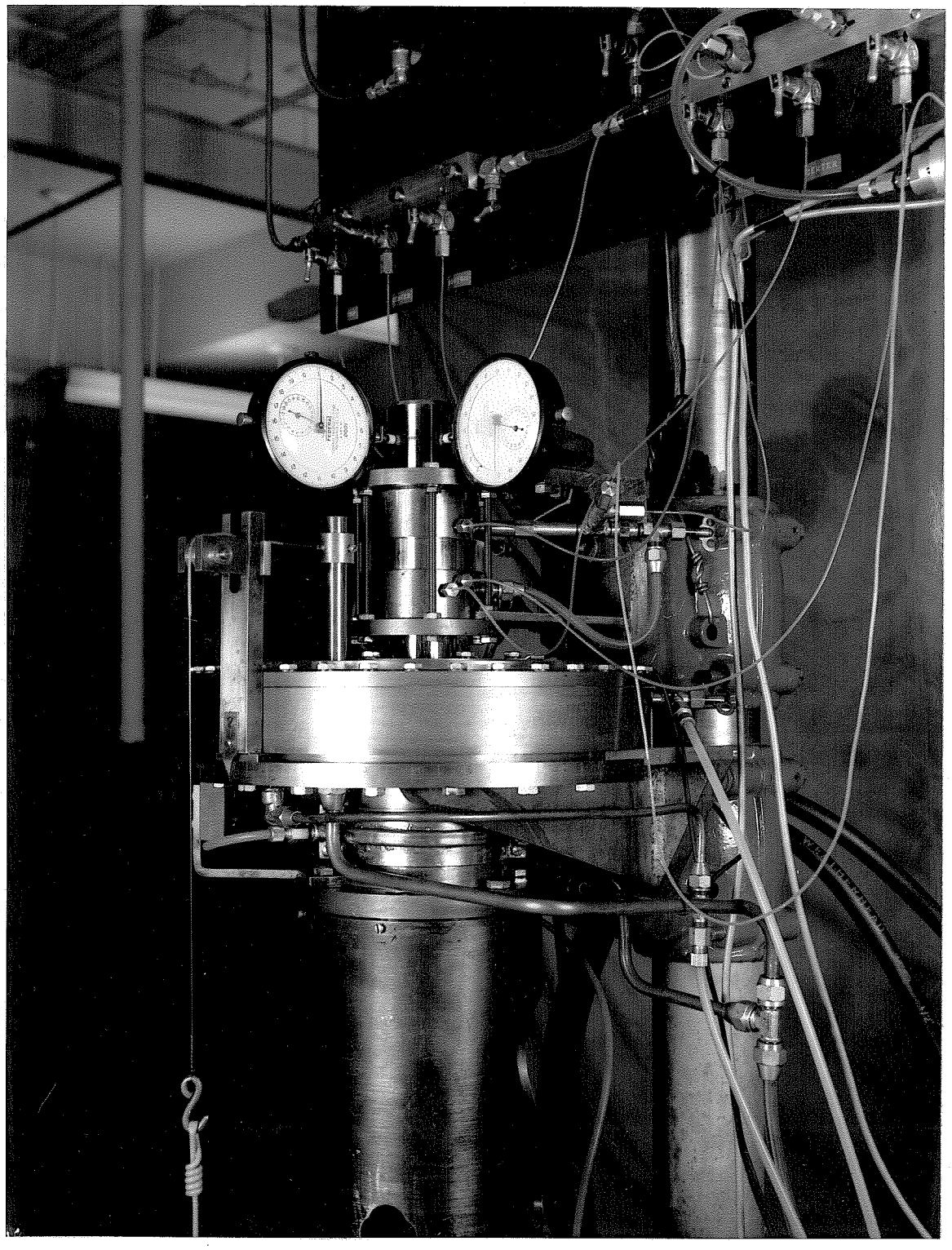

FIG. 6

TEST BEARING SECTION OF APPARATUS.

APPENDIX II: EXPERIMENTAL RESULTS

TABLE I

I.D. Measurements of Brass Bearing Used in Pressure Distribution Investigation.

Diameter in the direction of pressure taps (inches):

Measurement	First	Second	Third	Average
Top	2.0040	2.0041	2.0041	2.00407
Center	2.0040	2.0041	2.0041	2.00407
Bottom	2.0042	2.0042	2.0042	2.0042
				2.00413

Diameter in the direction normal to pressure taps:

Top	2.0040	2.0041	2.0041	2.00407
Center	2.0041	2.0040	2.0040	2.00403
Bottom	2.0042	2.0042	2.0042	2.0042
				2.0041

Average C = 0.00205

Maximum variation in C $= \frac{0.0001}{0.00205} .100$

= 4.9% of the gap.

TABLE II

I.D. Measurements of Lucite Bearing Used for Visual Observation of Oilfilm Behaviour

Diameter in direction I (inches):

	First Meas.	Second	Third	Average
Top	2.0035	2.0034	2.0035	2.00343
Center	2.0033	2.0034	2.0034	2.00336
Bottom	2.0034	2.0033	2.0034	2.00336
				2.00338

Diameter in direction II (perpendicular to direction I)

Top	2.0034	2.0034	2.0034	2.0034
Center	2.0034	2.0033	2.0033	2.00333
Bottom	2.0033	2.0033	2.0033	2.00333
				2.00335

Average C = 0.00168

Maximum variation in C $= \frac{0.0001}{0.000168} .100$

= 6% of the gap.

Test shaft measurements gave O.D. consistently as 2.0000 inches over the entire test section.

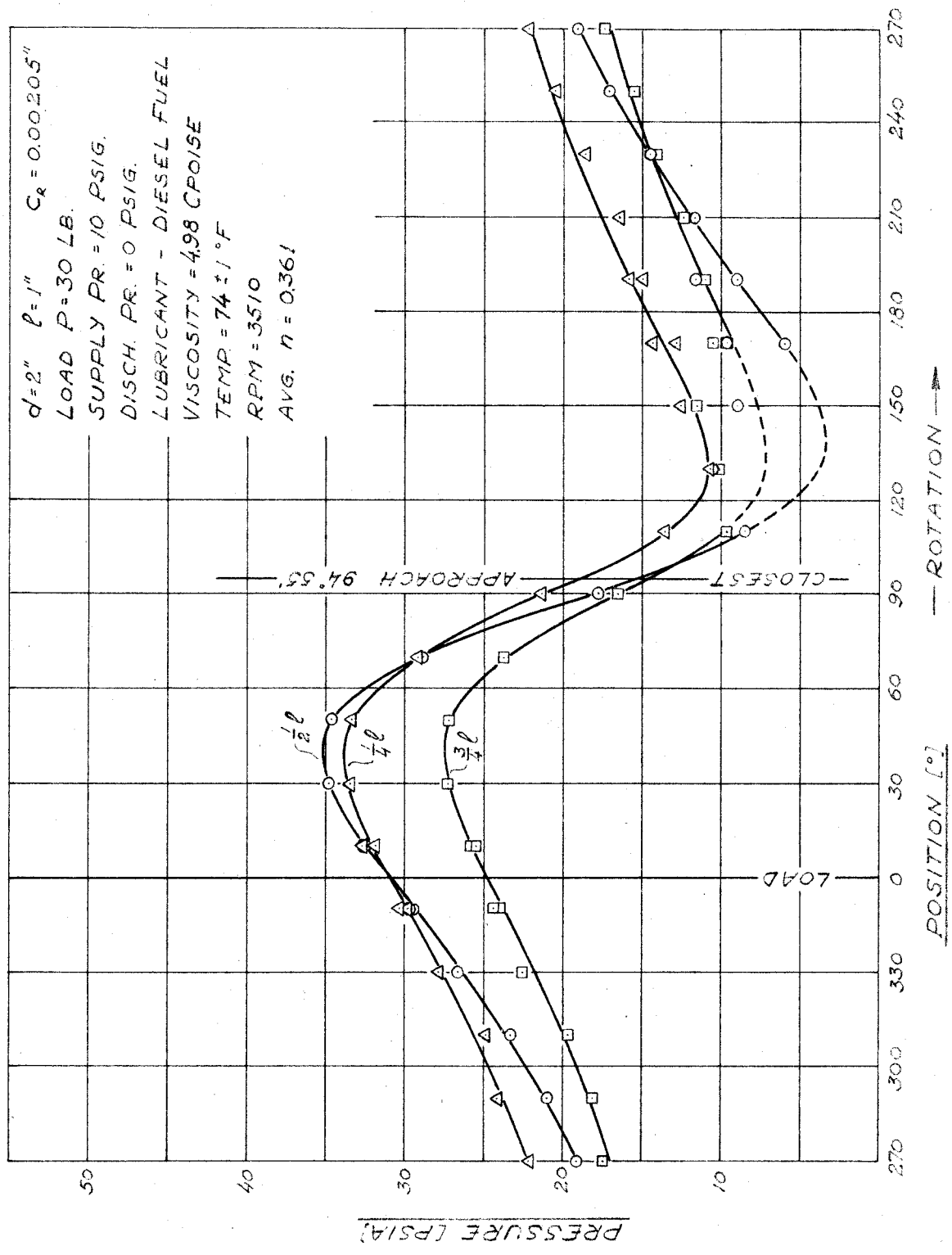

FIG. 7. TEST BEARING PRESSURE DISTRIBUTION WITH 30 LB. LOAD AND 10 PSI/IN AXIAL PRESSURE GRADIENT.

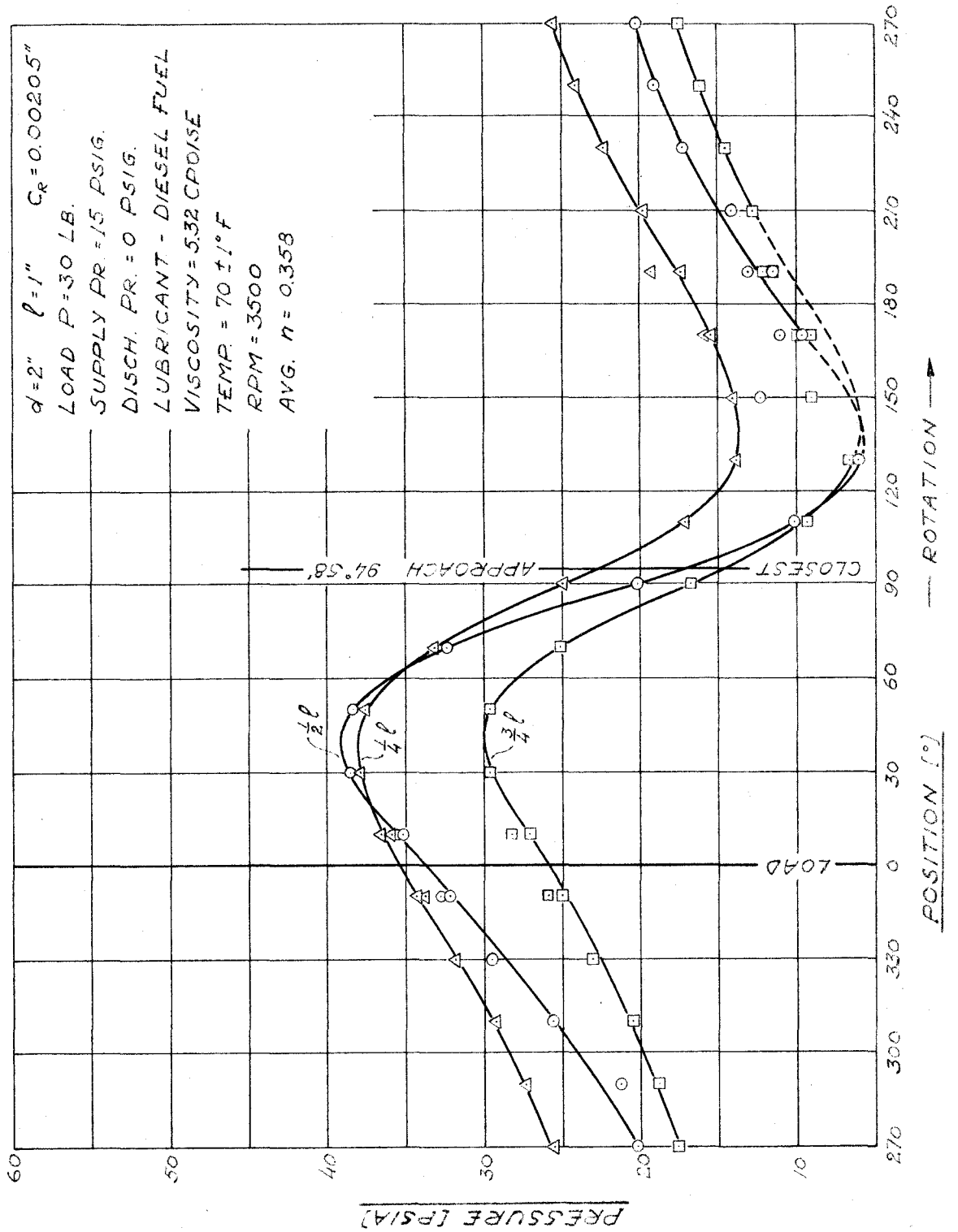

FIG. 8. TEST BEARING PRESSURE DISTRIBUTION WITH 30 LB. LOAD AND 15 PSI/IN AXIAL PRESSURE GRADIENT.

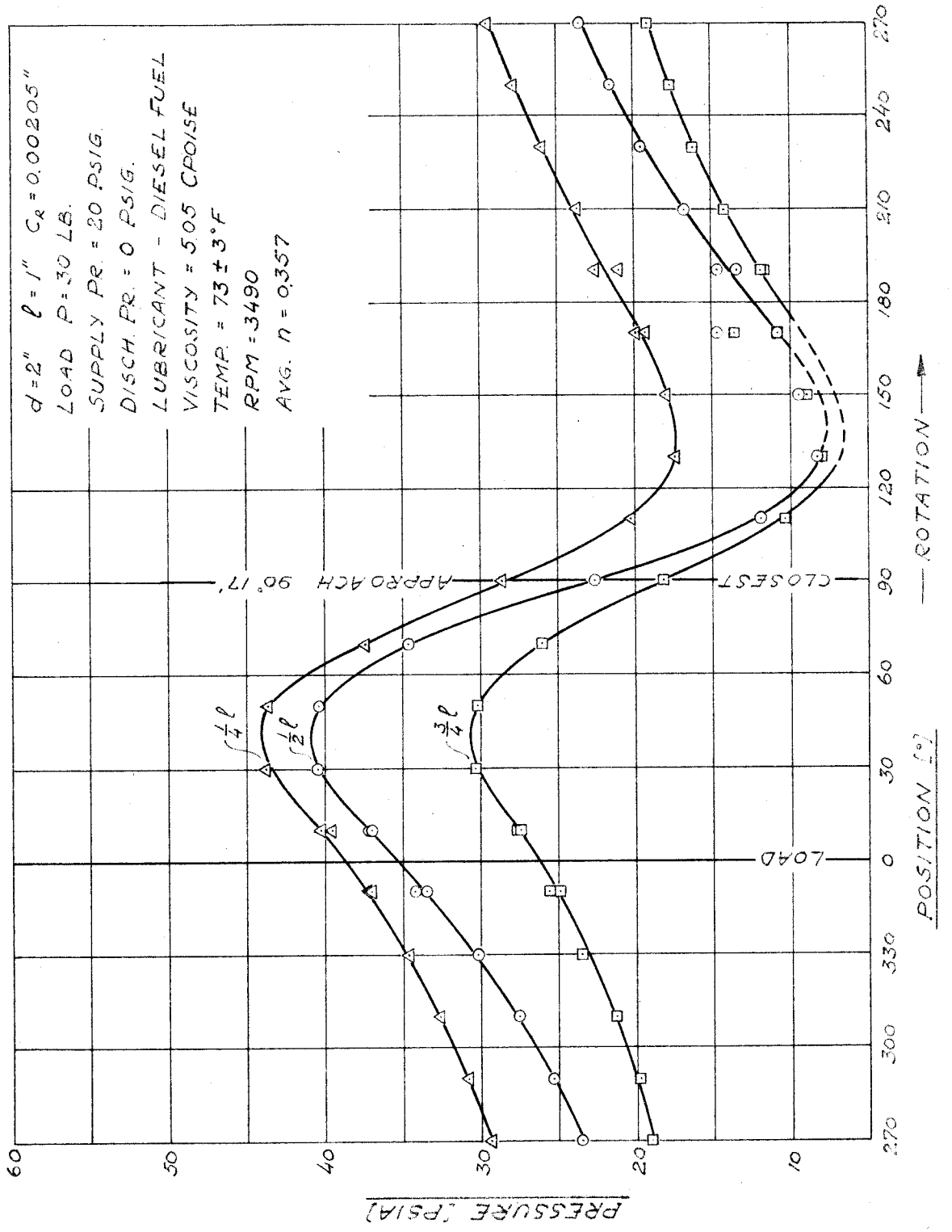

FIG. 9. TEST BEARING PRESSURE DISTRIBUTION WITH 30 LB. LOAD AND 20 PSI/IN AXIAL PRESSURE GRADIENT.

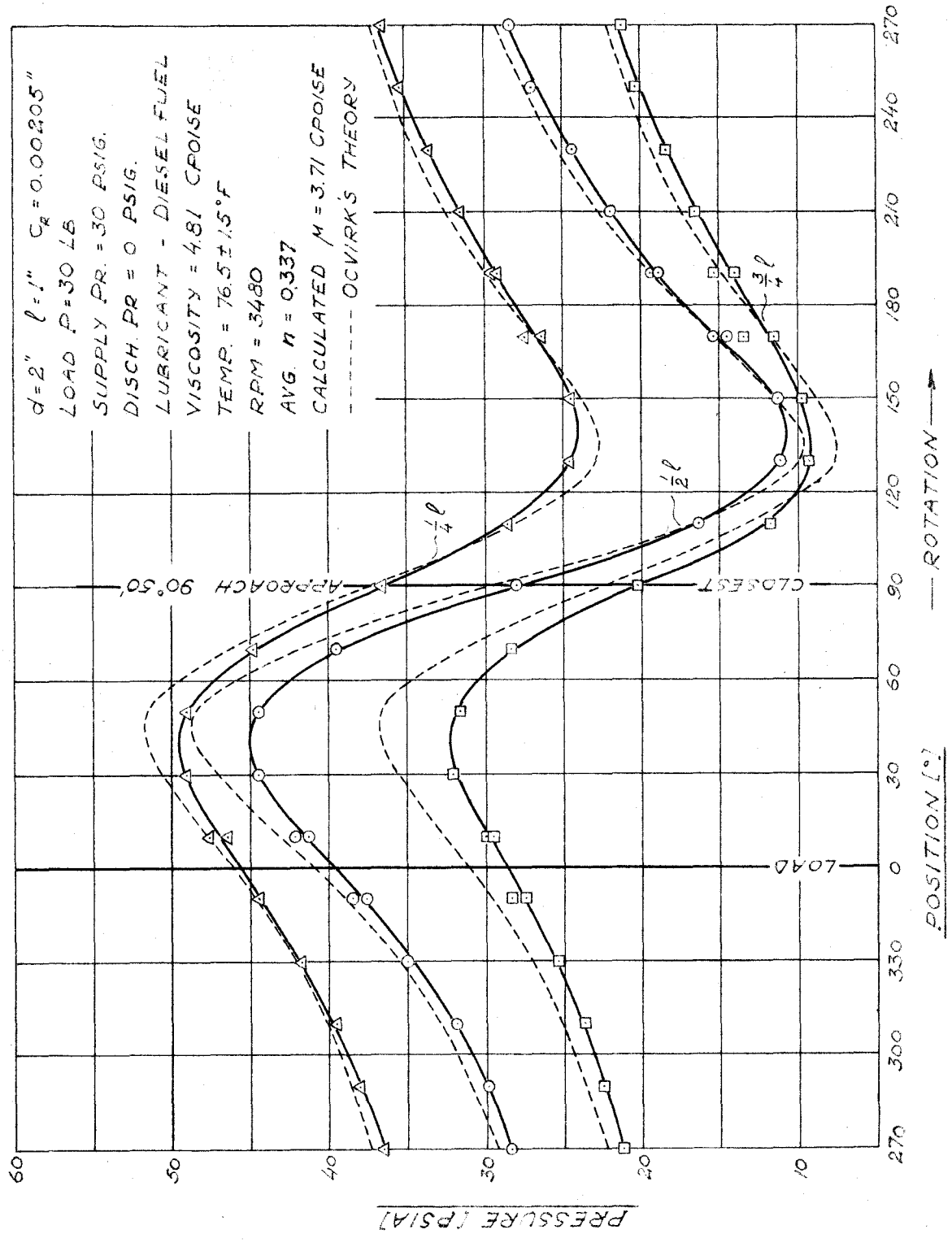

FIG. 10. TEST BEARING PRESSURE DISTRIBUTION WITH 30 LB. LOAD AND 30 PSI/IN AXIAL PRESSURE GRADIENT.

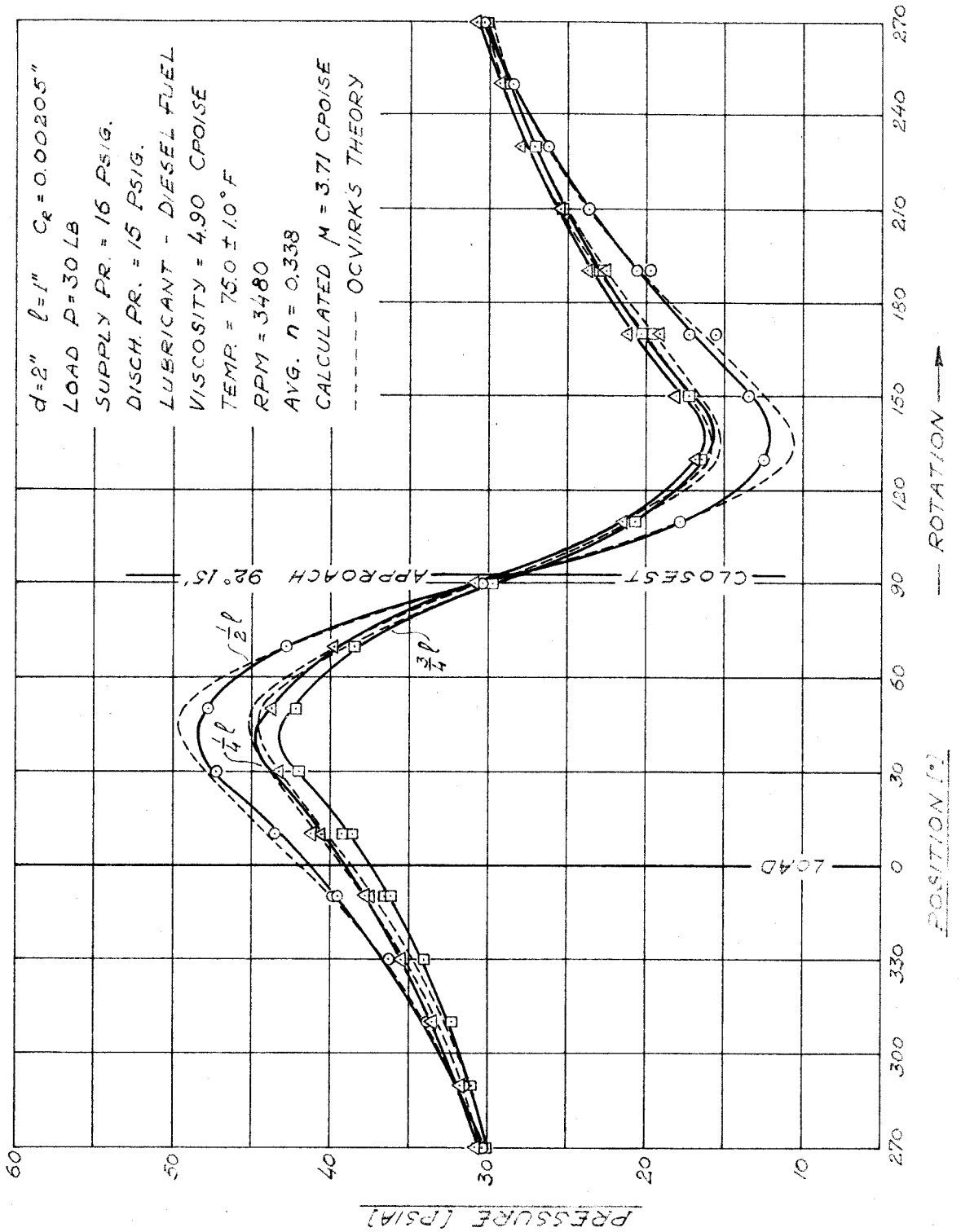

FIG. 11. TEST BEARING PRESSURE DISTRIBUTION WITH 30 LB. LOAD, 1 PSI/IN AXIAL PRESSURE GRADIENT AND 16 PSIG SUPPLY.

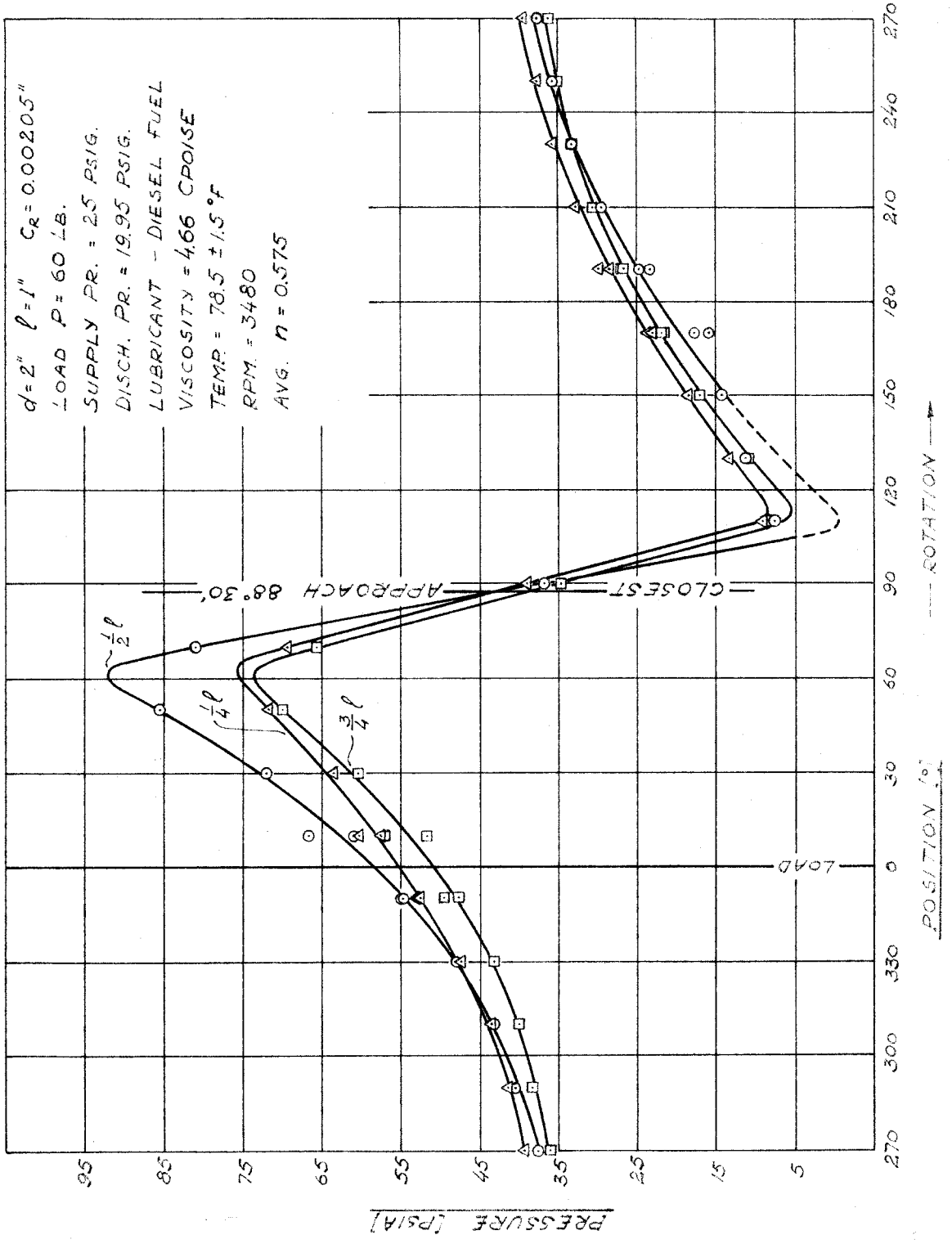

FIG. 12. TEST BEARING PRESSURE DISTRIBUTION WITH 60 LB. LOAD, 5 PSI/IN AXIAL PRESSURE GRADIENT AND 25 PSIG SUPPLY.

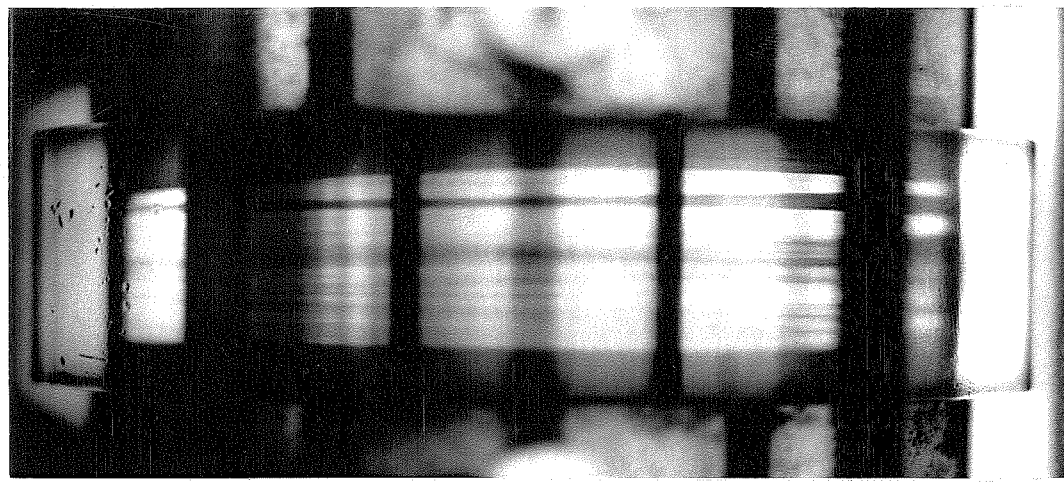

FIG. 13. CAVITATION IN JOURNAL BEARING OIL FILM.

Load - 60 lb.
Speed - 3530 rpm.
P_S = 4.3 psig.
P_D = 0 psig.
Cavity shape is stable.

n = 0.624
Φ = 76° 45'
Supply μ = 4.83 cpoise
Extent of cavity 90° to 350°

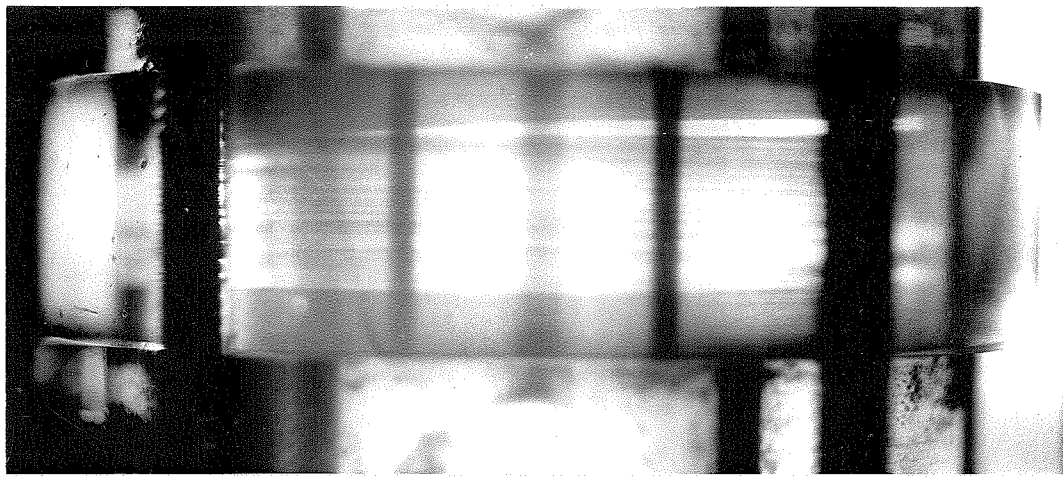

FIG. 14. CAVITATION IN JOURNAL BEARING OIL FILM.

Load - 60 lb.
Speed - 3530 rpm.
P_S = 5.0 psig.
P_D = 0 psig.
Cavity shape is stable.

n = 0.624
Φ = 76° 45'
Supply μ = 4.90 cpoise
Extent of cavity 110° to 340°

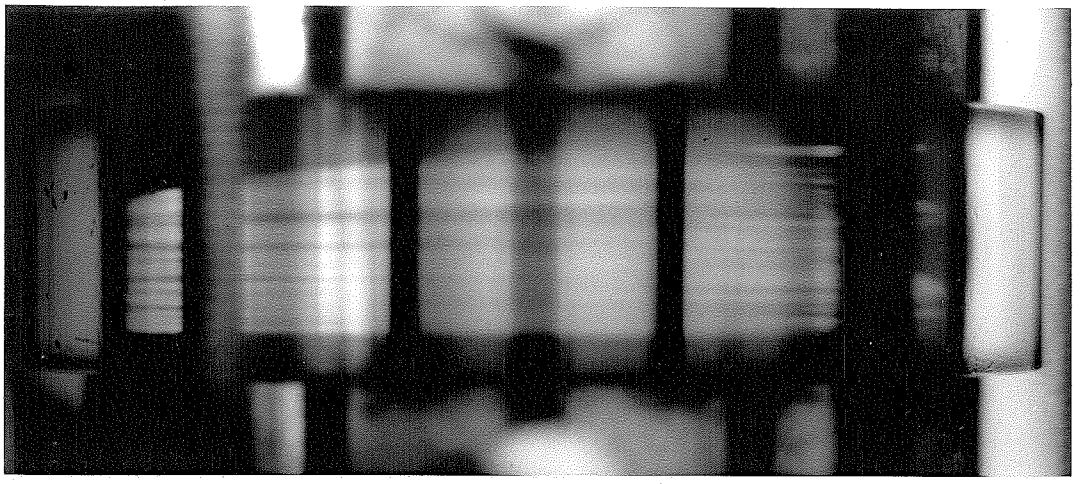

FIG. 15. CAVITATION IN JOURNAL BEARING OIL FILM.

Load - 60 lb.
Speed - 3530 rpm.
P_S = 6.5 psig.
P_D = 0 psig.
Top edge of cavity unstable.

n = 0.576
$\Phi = 82^\circ 52'$
Supply μ = 4.83 cpoise
Extent of cavity 100° to 340°

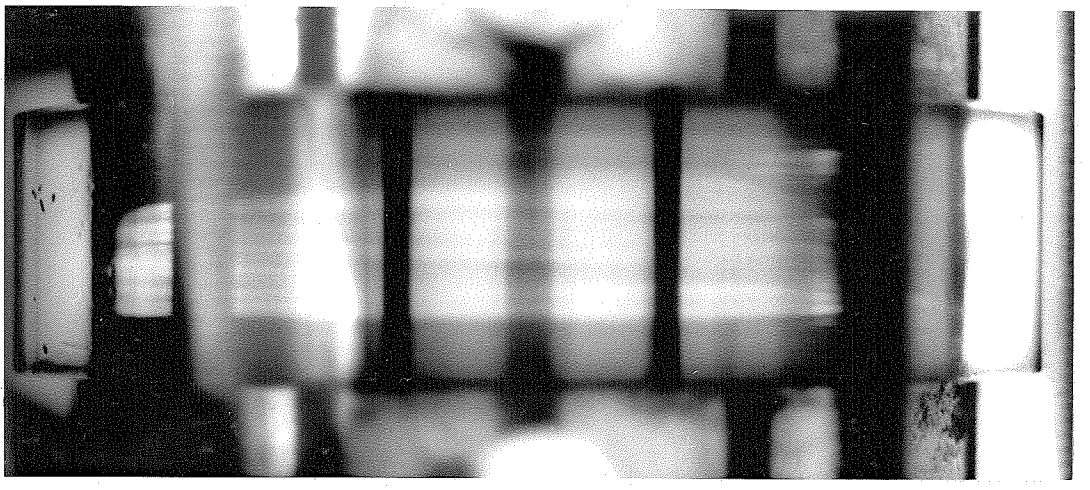

FIG. 16. CAVITATION IN JOURNAL BEARING OIL FILM.

Load - 60 lb.
Speed - 3480 rpm.
P_S = 8.8 psig.
P_D = 0 psig.
Shape of cavity unstable at the start. (see Fig. 17)

n = 0.47
$\Phi = 81^\circ 16'$
Supply μ = 4.75 cpoise
Extent of cavity 120° to 330°

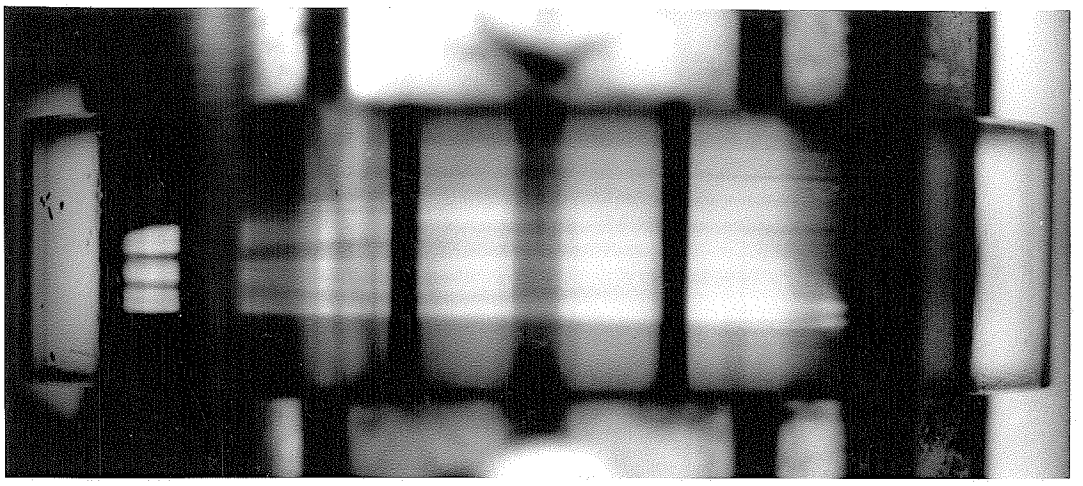

FIG. 17. CAVITATION IN JOURNAL BEARING OIL FILM.

Load - 60 lb.
Speed - 3480 rpm.
P_S = 8.8 psig.
P_D = 0 psig.
Shape of cavity unstable at the start. (see Fig. 16)

n = 0.47
$\Phi = 81^\circ 16'$
Supply μ = 4.75 cpoise
Extent of cavity 120° to 330°

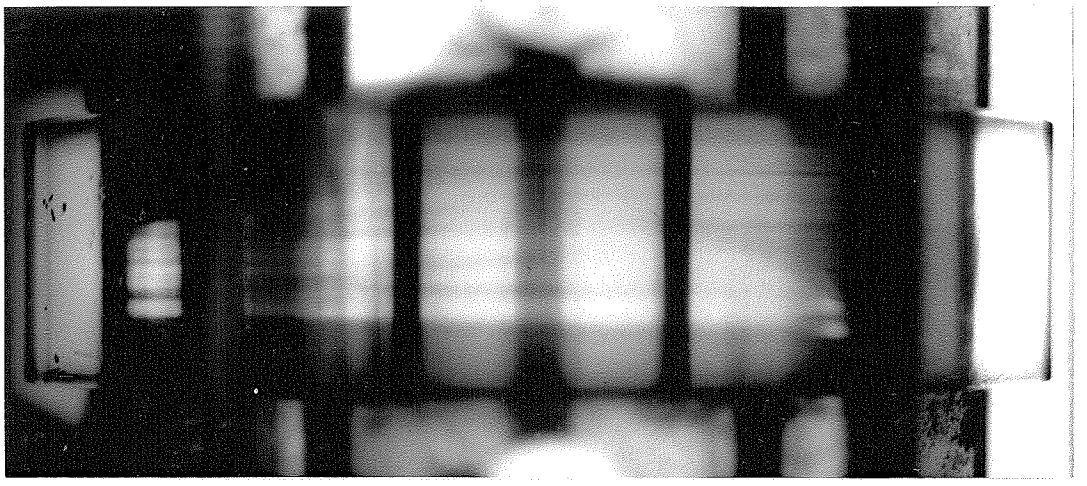

FIG. 18. CAVITATION IN JOURNAL BEARING OIL FILM.

Load - 60 lb.
Speed - 3470 rpm.
P_S = 10 psig.
P_D = 0 psig.
Partly unstable. (see Fig. 19)

n = 0.505
$\Phi = 98^\circ 8'$
Supply μ = 4.75 cpoise
Extent of cavity 120° to 310°

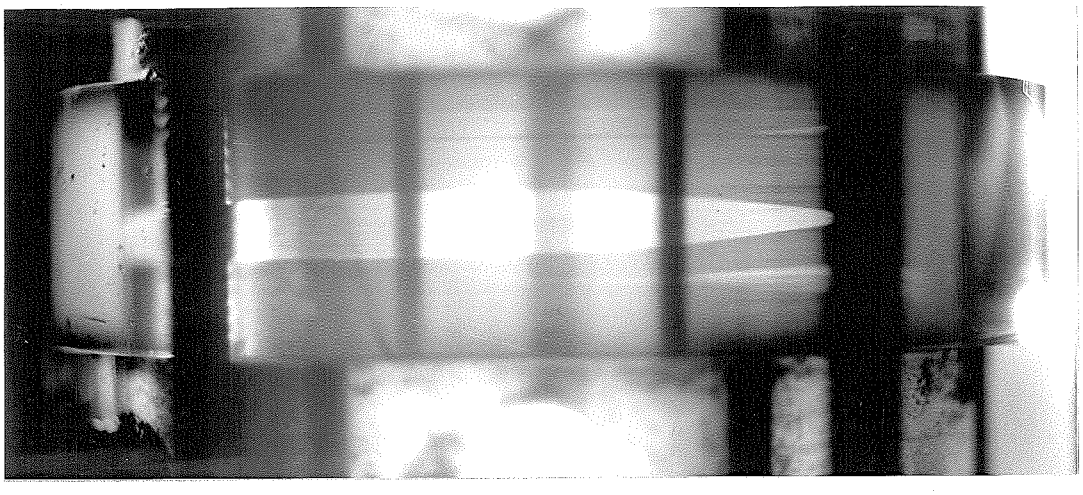

FIG. 19. CAVITATION IN JOURNAL BEARING OIL FILM.

Load - 60 lb.
Speed - 3510 rpm.
P_S = 10 psig.
P_D = 0 psig.
Partly unstable. (see Fig. 18)

n = 0.502
Φ = 94° 5'
Supply μ = 4.90 cpoise
Extent of cavity 130° to 290°

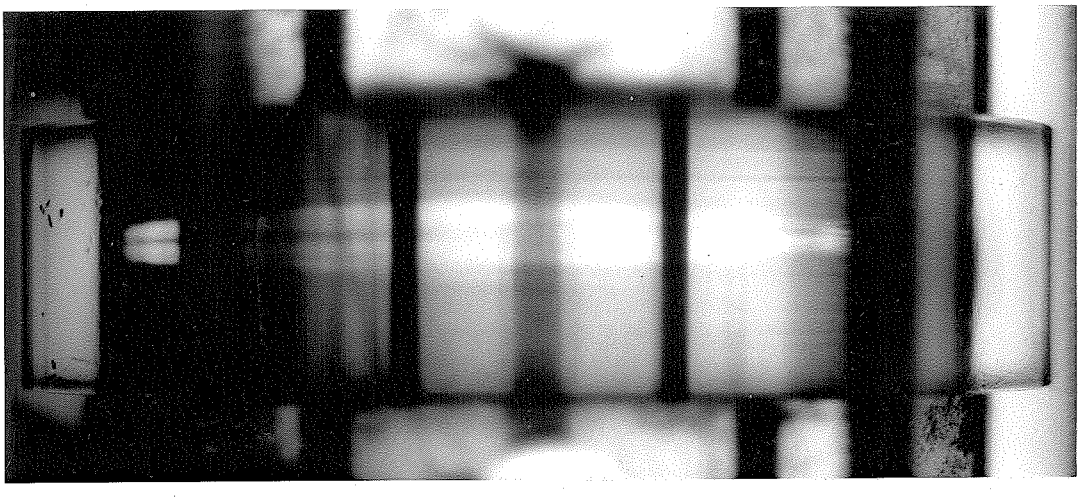

FIG. 20. CAVITATION IN JOURNAL BEARING OIL FILM.

Load - 60 lb.
Speed - 3470 rpm.
P_S = 11.8 psig.
P_D = 10 psig.
Cavity shape is unstable.

n = 0.505
Φ = 98° 8'
Supply μ = 4.75 cpoise
Extent of cavity 130° to 280°

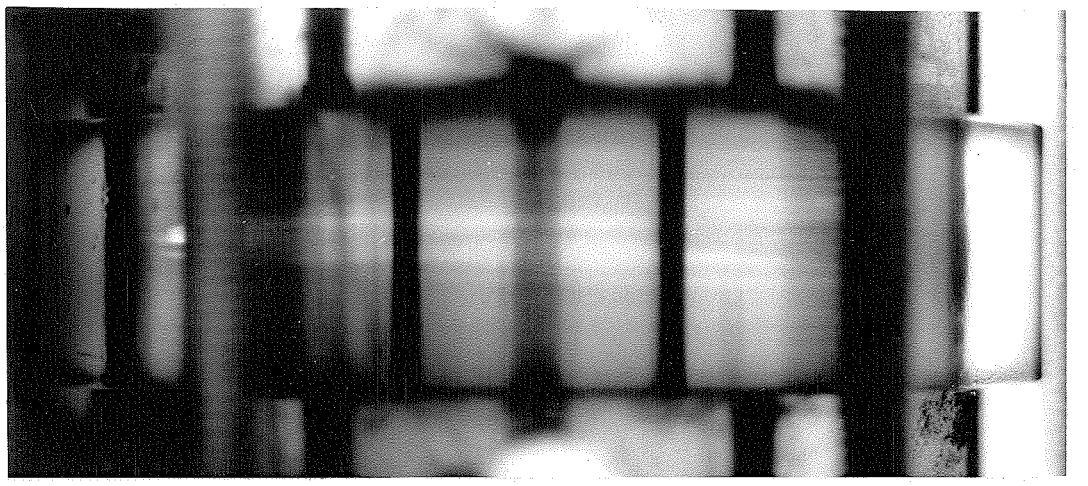

FIG. 21. CAVITATION IN JOURNAL BEARING OIL FILM.

Load - 60 lb.
Speed - 3470 rpm.
P_s = 12.7 psig.
P_D = 10.6 psig.
Cavity shape is unstable, tail end forms separate bubbles.

n = 0.505
Φ = 98° 8'
Supply μ = 4.70 cpoise
Extent of cavity 140° to 280° (310°)

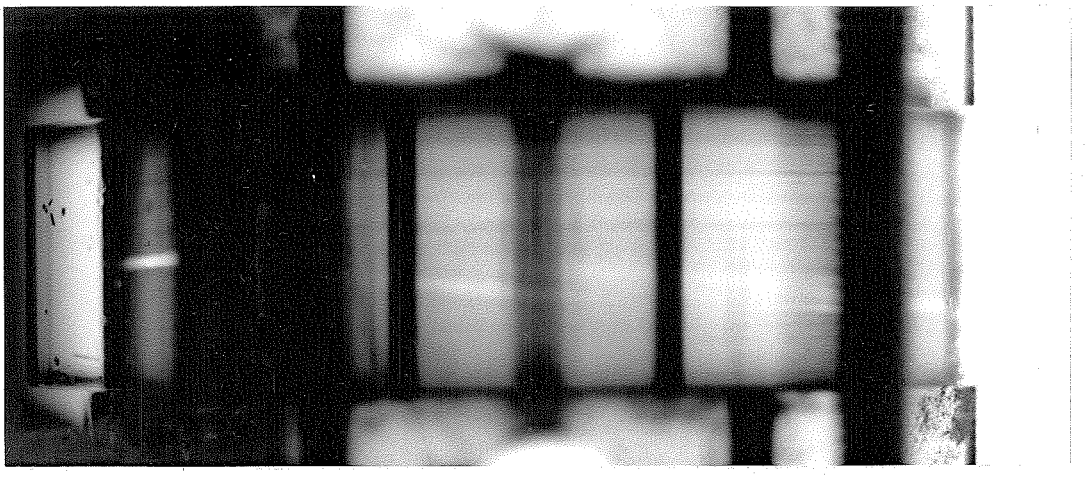

FIG. 22. CAVITATION IN JOURNAL BEARING OIL FILM.

Load - 60 lb.
Speed - 3465 rpm.
P_s = 14.3 psig.
P_D = 9.6 psig.

n = 0.47
Φ = 98° 40'
Supply μ = 4.70 cpoise
Extent of cavity 140° to 280°

Cavity is unstable, wanders axially and tail end forms separate bubbles which tend to be carried right through the high pressure region.

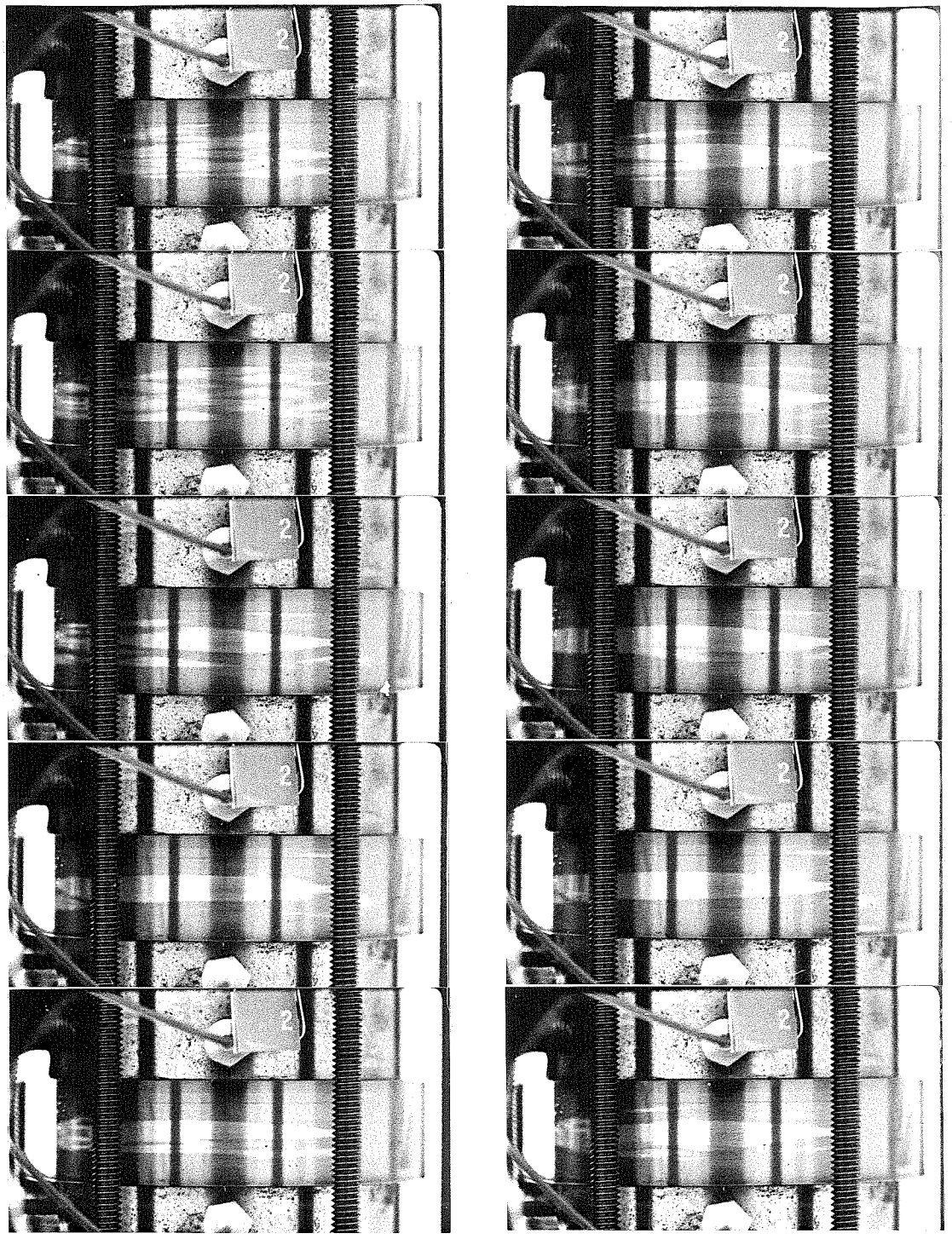

FIG. 23. CAVITATION IN JOURNAL BEARING OIL FILM.

Load - 60 lb.
Speed - 3510 rpm.
P_s = 7.8 psig.
P_D = 0 psig.
64 frames per sec. at 1/250 sec.

n = 0.505
$\Phi = 98^{\circ}\ 8'$
Supply μ = 5.08 cpoise

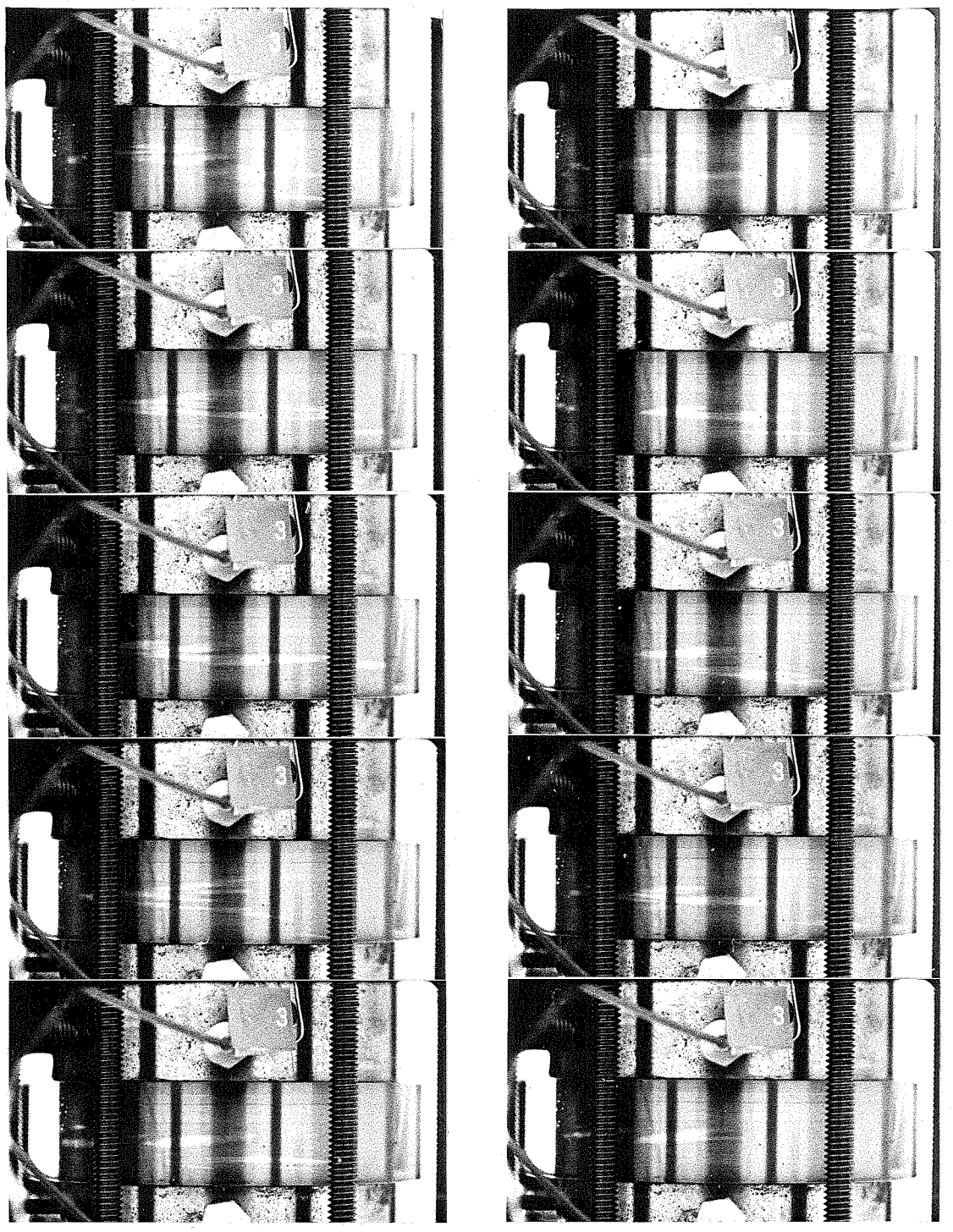

FIG. 24. CAVITATION IN JOURNAL BEARING OIL FILM.

Load - 60 lb.
Speed - 3420 rpm.
P_s = 8.7 psig.
P_D = 0 psig.

n = 0.47
Φ = 98° 40'
Supply μ = 5.08 cpoise

FIG. 25. CAVITATION IN JOURNAL BEARING OIL FILM.

Load - 60 lb.
Speed - 3440 rpm.
P_S = 10.8 psig.
P_D = 9.5 psig.

n = 0.435
$\Phi = 99^{\circ}\ 25'$
Supply μ = 4.91 cpoise

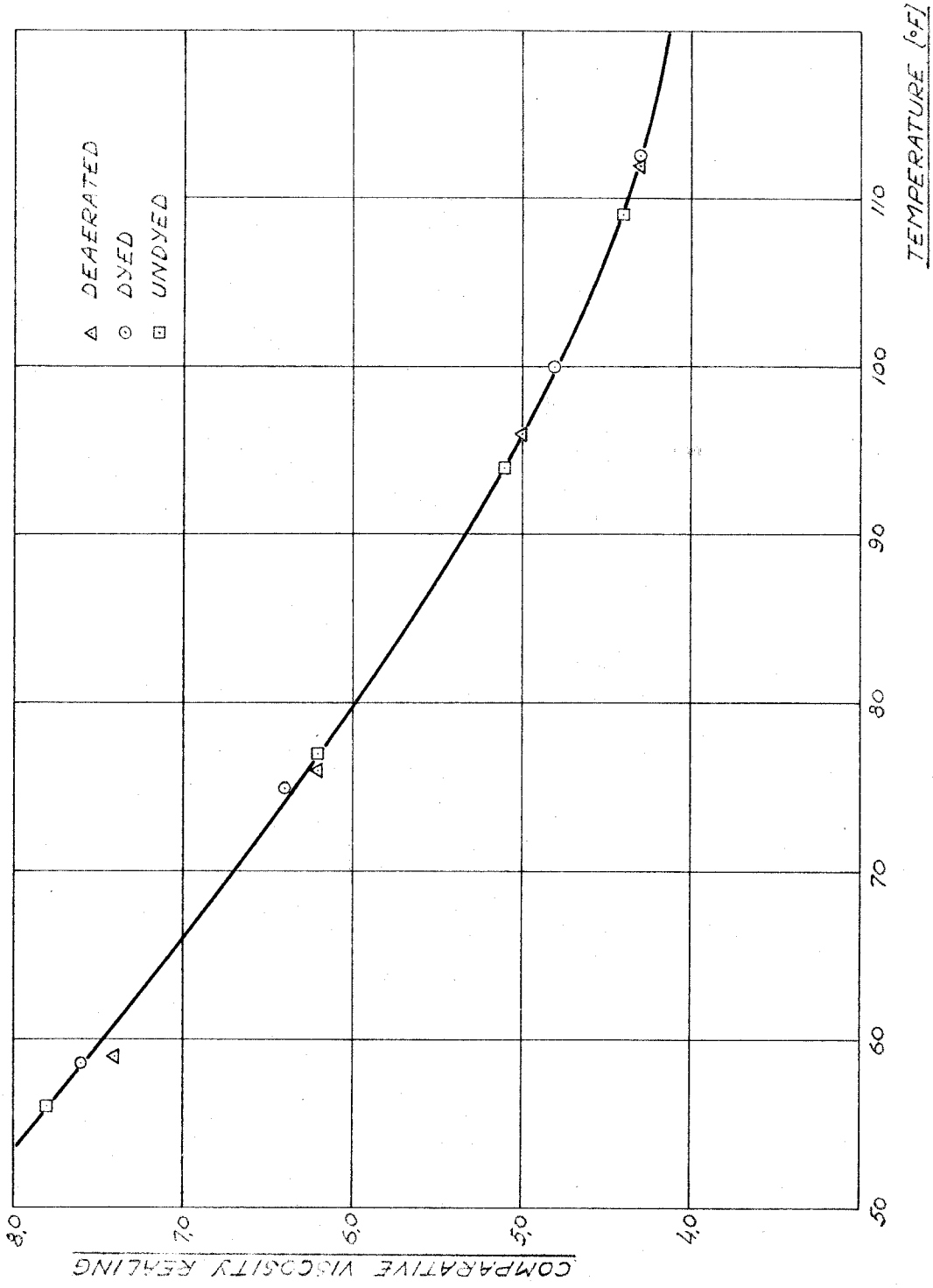

FIG. 26. COMPARATIVE VISCOSITIES OF DE-AERATED, DYED, AND UNDYED DIESEL FUEL.

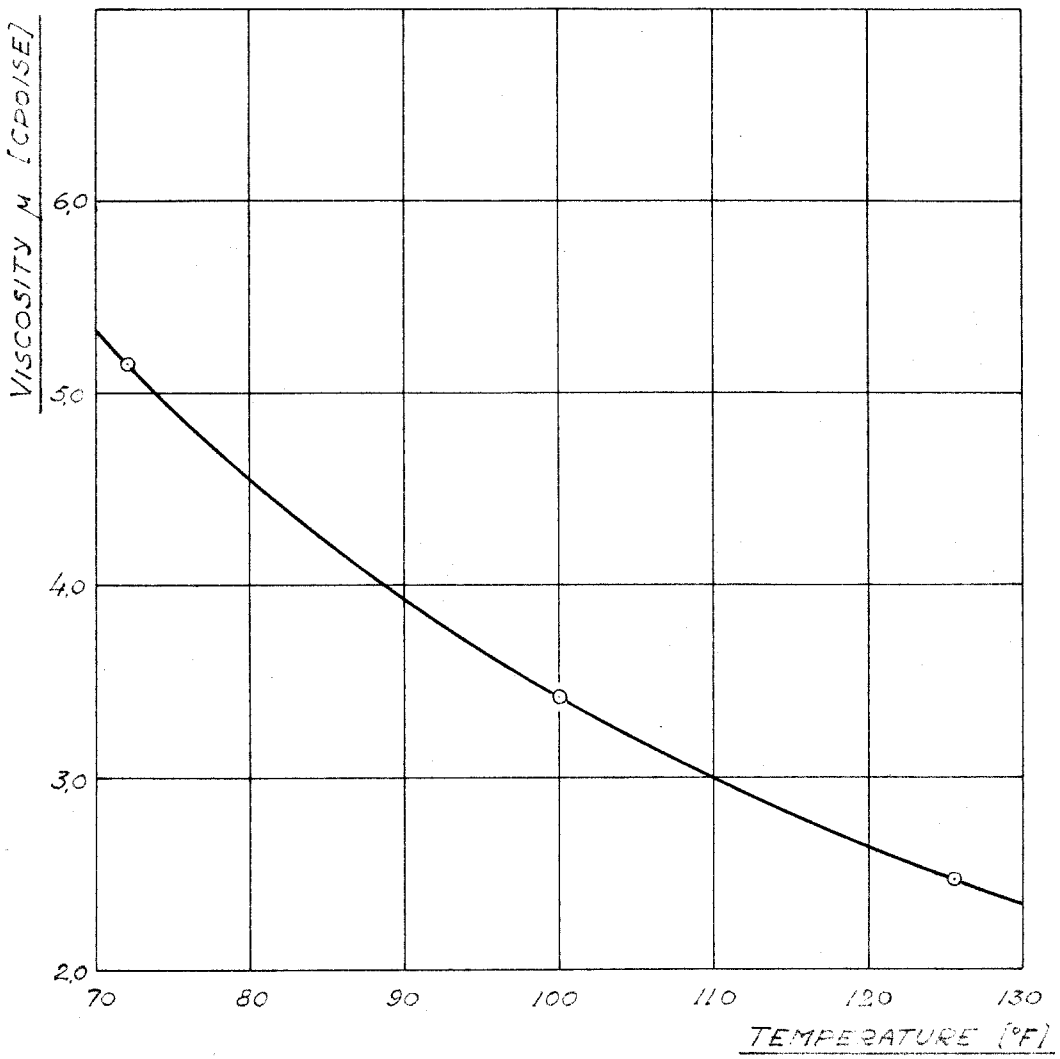

FIG. 27. VISCOSITY AS A FUNCTION OF TEMPERATURE FOR TEST BEARING LUBRICANT (DIESEL FUEL).

APPENDIX III: APPLICATION OF OCVIRK'S THEORY

OCVIRK'S SOLUTION AS APPLIED TO TEST BEARING.

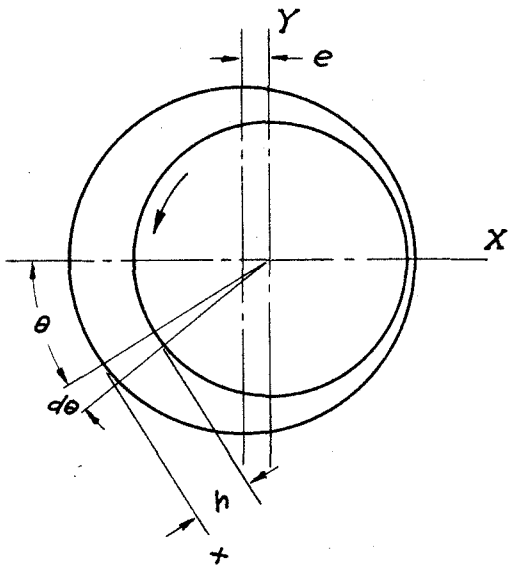

x = distance along the gap

h = local film thickness (gap)

z = axial coordinate

C_R = radial clearance

$n = e/C_R$

gap $h = C_R(1 + n\cos\theta)$

Reynold's Equation $\frac{\partial}{\partial x}\left(h^3\frac{\partial p}{\partial x}\right) + \frac{\partial}{\partial z}\left(h^3\frac{\partial p}{\partial z}\right) = 6\mu U\frac{\partial h}{\partial x}$

Ocvirk's approximate equation based on the assumption that circumferential pressure gradient effect on the flow is negligible

$$\frac{\partial}{\partial z}\left(h^3\frac{\partial p}{\partial z}\right) = 6\mu U\frac{\partial h}{\partial x}$$

Since h is independent of z we have:

$$\frac{d^2p}{dz^2} = \frac{6\mu U}{h^3}\frac{dh}{dx}$$

Solution is: $$p = \frac{6\mu U}{h^3}\frac{dh}{dx}\frac{z^2}{2} + C_1 z + C_2$$

Measuring axial distance from supply plenum we have boundary conditions:

$p = P_s$ at $z = 0$

$p = P_o$ at $z = \ell$

Applying boundary conditions we get:

$$C_2 = P_s \qquad C_1 = \frac{P_o - P_s}{\ell} - \frac{6\mu U}{h^3}\frac{dh}{dx}\frac{\ell}{2}$$

$\therefore$ For test bearing $\quad p = \frac{3\mu U}{h^3}\frac{dh}{dx}(z^2 - \ell z) + (P_D - P_S)\frac{z}{\ell} + P_S$

Changing to polar coordinates: $\quad dx = r\,d\theta \qquad \frac{dh}{dx} = \frac{1}{r}\frac{dh}{d\theta}$

$$\frac{dh}{d\theta} = -C_R n \sin\theta$$

Substitution gives:

$$p = \frac{3\mu U}{r C_R^2}(\ell z - z^2)\frac{n\sin\theta}{(1+n\cos\theta)^3} - (P_S - P_D)\frac{z}{\ell} + P_S \qquad \text{Eq. 1}$$

Considering the case of no cavitation we obtain load components in X and Y direction by integration over the length and the circumference of the journal.

$$P_X = -\int_0^{2\pi}\int_0^{\ell} p\, r\cos\theta\, d\theta\, dz$$

$$= -\int_0^{2\pi}\int_0^{\ell}\left\{\frac{3\mu U}{r C_R^2}(\ell z - z^2)\frac{n\sin\theta}{(1+n\cos\theta)^3} - (P_S - P_D)\frac{z}{\ell} + P_S\right\} r\cos\theta\, d\theta\, dz$$

$$= -\int_0^{2\pi}\left\{\frac{3\mu U}{r C_R^2}\left[\ell\frac{z^2}{2} - \frac{z^3}{3}\right]_0^{\ell}\frac{n\sin\theta}{(1+n\cos\theta)^3} - (P_S - P_D)\left[\frac{z^2}{2\ell}\right]_0^{\ell} + P_S z\right]_0^{\ell}\right\} r\cos\theta\, d\theta$$

$$= -\int_0^{2\pi}\frac{3\mu U}{r C_R^2}\frac{\ell^3 r}{6}\frac{n\sin\theta\cos\theta\, d\theta}{(1+n\cos\theta)^3} + \int_0^{2\pi}\left[(P_S - P_D)\frac{\ell}{2} - P_S\ell\right] r\cos\theta\, d\theta$$

$$= -\int_0^{2\pi}\frac{\mu U \ell^3}{2C_R^2}\frac{n\sin\theta\cos\theta}{(1+n\cos\theta)^3}\, d\theta - (P_S + P_D)\frac{\ell}{2} r \underbrace{[\sin\theta]_0^{2\pi}}_{=0}$$

$$= -\frac{\mu U \ell^3}{2C_R^2}\int_0^{2\pi}\frac{n\sin\theta\cos\theta}{(1+n\cos\theta)}\, d\theta$$

Evaluating the integral:

$$\int_0^{2\pi}\frac{n\sin\theta\cos\theta}{(1+n\cos\theta)^3}\, d\theta = \left[\frac{1}{n(1+n\cos\theta)}\right]_0^{2\pi} - \left[\frac{1}{2n(1+n\cos\theta)^2}\right]_0^{2\pi} = 0$$

as worked out by Ocvirk

$\therefore$ $P_X = 0$ for no cavitation $\qquad$ Eq. 2

$$P_Y = \int_0^{2\bar{\pi}} \int_0^{\ell} p\, r \sin\theta \, d\theta \, dz$$

$$= \int_0^{2\bar{\pi}} \int_0^{\ell} \left\{ \frac{3\mu U}{r C_R^2} (\ell z - z^2) \frac{n \sin\theta}{(1+n\cos\theta)^3} - (P_S - P_0)\frac{z}{\ell} + P_S \right\} r \sin\theta \, d\theta \, dz$$

$$= \int_0^{2\bar{\pi}} \frac{\mu U \ell^3}{2 C_R^2} \frac{n \sin^2\theta}{(1+n\cos\theta)^3} d\theta - \int_0^{2\bar{\pi}} \left[(P_S - P_0)\frac{\ell}{2} - P_S \right] r \sin\theta \, d\theta$$

$$= \int_0^{2\bar{\pi}} \frac{\mu U \ell^3}{2 C_R^2} \frac{n \sin^2\theta}{(1+n\cos\theta)^3} d\theta + (P_S + P_0)\frac{\ell}{2} r \left[-\cos\theta \right]_0^{2\bar{\pi}}$$

$$= \frac{\mu U \ell^3}{2 C_R^2} \int_0^{2\bar{\pi}} \frac{n \sin^2\theta}{(1+n\cos\theta)^3} d\theta$$

Evaluating the integral:

$$\int_0^{2\bar{\pi}} \frac{n \sin^2\theta}{(1+n\cos\theta)^3} d\theta = \left[-\frac{\alpha}{2n(1-n^2)^{1/2}} \right]_0^{2\bar{\pi}} + \frac{1}{2n(1-n^2)^{3/2}} \left[\alpha - n\sin\alpha \right]_0^{2\bar{\pi}}$$

as worked out by Ocvirk

$$= -\frac{2\bar{\pi}}{2n(1-n^2)^{1/2}} + \frac{2\bar{\pi}}{2n(1-n^2)^{3/2}}$$

$$= \frac{-\bar{\pi} + n^2\bar{\pi} + \bar{\pi}}{n(1-n^2)^{3/2}}$$

$$= \frac{\bar{\pi} n}{(1-n^2)^{3/2}}$$

$$\therefore P_Y = P = \frac{\mu U \ell^3}{2 C_R^2} \frac{n\bar{\pi}}{(1-n^2)^{3/2}} \quad \text{for no cavitation} \qquad \text{Eq. 3}$$

Attitude angle:

$$\phi = \tan^{-1}\frac{P_Y}{P_X} = \tan^{-1}\infty = 90^\circ$$